

Effects of nonmagnetic impurities and subgap states on the kinetic inductance, complex conductivity, quality factor and depairing current density

Takayuki Kubo*

*High Energy Accelerator Research Organization (KEK), Tsukuba, Ibaraki 305-0801, Japan and
The Graduate University for Advanced Studies (Sokendai), Hayama, Kanagawa 240-0193, Japan*

We investigate how a combination of a nonmagnetic-impurity scattering rate γ and finite subgap states parametrized by Dynes Γ affects various physical quantities relevant to superconducting devices: kinetic inductance L_k , complex conductivity σ , surface resistance R_s , quality factor Q , and depairing current density J_d . All the calculations are based on the Eilenberger formalism of the BCS theory. We assume the device materials are extreme type-II s -wave superconductors. It is well known that the optimum impurity concentration ($\gamma/\Delta_0 \sim 1$) minimizes R_s . Here, Δ_0 is the pair potential for the idealized ($\Gamma \rightarrow 0$) superconductor for the temperature $T \rightarrow 0$. We find the optimum Γ can also reduce R_s by one order of magnitude for a clean superconductor ($\gamma/\Delta_0 < 1$) and a few tens % for a dirty superconductor ($\gamma/\Delta_0 > 1$). Also, we find a nearly-ideal ($\Gamma/\Delta_0 \ll 1$) clean-limit superconductor exhibits a frequency-independent R_s for a broad range of frequency ω , which can significantly improve Q of a very compact cavity with a few tens of GHz frequency. As Γ or γ increases, the plateau disappears, and R_s obeys the ω^2 dependence. The subgap-state-induced residual surface resistance R_{res} is also studied, which can be detected by an SRF-grade high- Q 3D resonator. We calculate $L_k(\gamma, \Gamma, T)$ and $J_d(\gamma, \Gamma, T)$, which are monotonic increasing and decreasing functions of (γ, Γ, T) , respectively. Measurements of (γ, Γ) of device materials can give helpful information on engineering (γ, Γ) via materials processing, by which it would be possible to improve Q , engineer L_k , and ameliorate J_d .

I. INTRODUCTION

The microscopic theory of superconductivity is the linchpin of research and development of various superconducting devices, such as superconducting radio-frequency (SRF) cavities for particle accelerators [1–3], superconducting magnets and cables [4], kinetic inductance detectors (KID) [5], hot-electron bolometer [6], other superconducting instruments for astrophysics and cosmology [7], superconducting single-photon detectors (SSPD) [8, 9], and superconducting qubit for quantum information processing (QIP) [10, 11]. Models of superconducting devices based on the idealized BCS superconductor without any pair breakers usually provide good starting points to understand the operating principles of these technologies. However, such models are sometimes too naive to analyze the physics of real devices. The representative example is the quality factor Q of superconducting resonators. The surface resistance and then Q are sensitive to the detail of the quasiparticle density of states (DOS), which is affected by various pair breakers in the real world, such as the current and magnetic impurities [12–16]. Hence, an analysis of Q based on the ideal BCS DOS, i.e., the Mattis-Bardeen (MB) theory [17], is qualitative and sometimes inadequate even for qualitative analyses. In fact, the MB theory cannot explain the rf-field dependent nonlinear Q , effects of material-treatment on Q , and saturation of Q at $T \rightarrow 0$. Another example is the depairing current density J_d . The well-known Kupriyanov-Lukichev-Maki theory [18, 19] gives

J_d for the ideal BCS superconductor. However, pair-breakers in device materials (e.g., magnetic impurities) can degrade J_d and thus reduce the ultimate limit of the current density in superconducting cables and that of the accelerating field of the SRF cavity [20]. To understand the physics of superconducting devices and to discern the causes of unexpected performance limitations of real devices, we need to take various pair-breakers in real materials into account (e.g., current, magnetic impurities, metallic suboxides, hydride, and non-stoichiometric regions) and to assess the effects of such non-ideal features on device performances [21, 22].

One of the non-ideal features observed in various superconducting materials is the broadening and subgap states in DOS [23–29], in contrast to the sharp spectrum gap in the idealized BCS superconductor. Various mechanisms can contribute to the subgap states, e.g., inelastic scattering of quasiparticles on phonons [30], Coulomb correlations [31], anisotropy of the Fermi surface [32], local inhomogeneities of the BCS pairing constant [33], magnetic impurities [34], and effects of spatial correlations in impurity scattering [35]. Such a broadened DOS is often described by using the phenomenological Dynes formula [36, 37], $N(\epsilon)/N_0 = \text{Re}[(\epsilon + i\Gamma)/\sqrt{(\epsilon + i\Gamma)^2 - \Delta^2}]$ (see Fig. 1). Here Δ is the pair potential, N_0 is the normal-state DOS at the Fermi level, and Γ is the Dynes broadening parameter. We can reproduce the ideal BCS-DOS by taking $\Gamma \rightarrow 0$. Irrespective of microscopic models of the Dynes formula, we can incorporate Γ into the quasiclassical formalism of the BCS theory (see e.g., Refs. [21, 22, 38–41]). Also, microscopic derivations of the Dynes formula have been investigated [42, 43].

The first way to calculate physical quantities based on realistic spectrum is to incorporate all the broadening

* kubotaka@post.kek.jp; Stay-at-home dad on two-year paternity leave, New York, NY, USA

mechanisms in materials into a device model. However, such a model should contain a bunch of free parameters and practically useless unless those parameters are determined from a number of experiments. Another way is to introduce the phenomenological Dynes Γ into a device model. Here, a value of Γ can be determined from experiments such as tunneling spectroscopy [23] and measurements of complex conductivity [44, 45]. Even if we do not know what kind of pair breakers contribute to sub-gap states, such an experimentally determined Γ makes it possible to calculate physical quantities based on the realistic quasiparticle spectrum. In the present paper, we pursue the second approach, which would give reliable results rather than those based on the idealized BCS-DOS.

According to the previous studies for the diffusive limit [21, 22, 38, 39], influences of a finite Γ is far-reaching: it affects, e.g., the pair potential Δ , the critical temperature T_c , the penetration depth λ , the kinetic inductivity L_k , the complex conductivity σ , the coherence peak of dissipative-conductivity σ_1 , the surface impedance, Q factor, and the depairing current density J_d . One of the nontrivial consequences is the fact that there exists the optimum Γ , which maximizes Q at some temperature range [3, 21, 22, 38]. This Γ -induced Q -rise comes from the same mechanism as the Q rise due to current-induced DOS broadening [46, 47]. On the other hand, finite subgap states in the vicinity of the Fermi level induce a residual dissipative conductivity $\lim_{T \rightarrow 0} \sigma_1$ [2, 3, 21, 38, 48].

The effects of a finite Γ in a moderately clean superconductor have been studied less extensively except for some calculations of σ [44, 48]. In the present study, we investigate the effects of a combination of Dynes Γ and nonmagnetic-impurity scattering rate γ on the kinetic inductivity L_k , the surface resistance R_s , and the depairing current density J_d , which are the physical quantities relevant to modern superconducting devices. The kinetic inductance is known to limit the reset time after a detection event of SSPD [49] and also plays an essential role in the operating mechanism of KID, which detects a shift of resonant frequency $\delta f \propto -\delta L_k$ due to the arrival of pair-breaking photons [5]. The surface resistance R_s is proportional to the dissipation at the inner surface of a 3D resonant cavity for SRF and QIP. Reduction of R_s (or improvement of Q) has been the primary interest of researchers of resonant cavities over the last decades. Vortex-free Nb cavities [50–55] exhibit huge quality factor $Q \sim 10^{10}$ - 10^{12} at $T < 2$ K [56–59] even under the strong rf current [60–63] close to the depairing current density. The depairing current density J_d is related to the bias current of SSPD and is the maximum current that SRF cavities and superconducting cables can support. The screening current density on the inner surface of the cutting-edge Nb cavity reaches a current density close to J_d , and SRF researchers study next-generation cavities using alternative materials with higher J_d theoretically [64–69] and experimentally [70–80].

Our calculations are based on the well-established

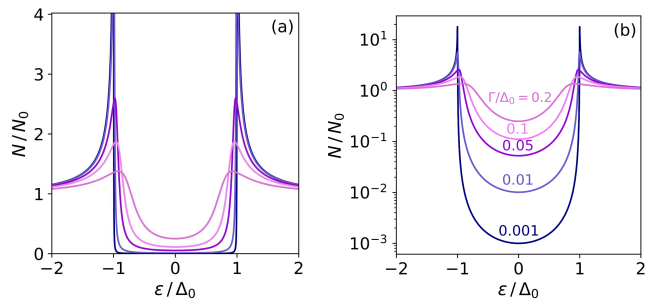


FIG. 1. (a) Quasiparticle density of states (DOS) at $T \rightarrow 0$ calculated for $\Gamma/\Delta_0 = 0.2, 0.1, 0.05, 0.01$, and 0.001 . (b) DOS in a logarithmic scale. Note DOS in the zero-current state is independent of a concentration of nonmagnetic impurities.

Eilenberger formalism of the BCS theory [16, 81], which can include an arbitrary impurity concentration. We assume that the penetration depth λ is much larger than the coherence length ξ , then a superconductor obeys the local electrodynamics. Large- λ/ξ superconductors include dirty Nb and also NbN, NbTiN, and Nb₃Sn for any impurity concentration from the clean limit to the dirty limit.

The paper is organized as follows. In Section II, we briefly review the Eilenberger formalism of the BCS theory [16, 81] and basic consequences of a finite Γ in the zero-current state. In Sec. III, we evaluate the penetration depth $\lambda(\gamma, \Gamma, T)$ and the kinetic inductivity $L_k(\gamma, \Gamma, T)$. Convenient formulas for λ and L_k are also summarized. In Sec. IV, we summarize the complex conductivity formulas, evaluate the T dependence and the coherence peak, and consider the low T limit and moderately low T regime ($\hbar\omega \ll k_B T \ll \Delta_0$). Then, combining the results of Sec. III and Sec. IV A - IV D, we study the effects of (γ, Γ) on the surface resistance and Q factor in the low T limit and the moderately-low T regime. In Sec. V, we solve the Eilenberger equation in the current-carrying state and evaluate the effects of (γ, Γ) on the depairing current density J_d . In Sec. VI, we discuss the implications of our results.

II. THEORY

A. Eilenberger equation

The normal (g_m) and anomalous (f_m) quasiclassical Matsubara Green's functions obey the Eilenberger equation [16, 81]. Since we consider the case $\lambda \gg \xi$, the current distribution varies slowly over the coherence length, and then the spatial-differentiation terms are negligible. The Eilenberger equation for the current-carrying state

reduces to

$$\left[i\frac{\pi s}{2} \cos \theta + (\hbar\omega_m + \Gamma) \right] f_m - \Delta g_m = \gamma \{ \langle f_m \rangle g_m - \langle g_m \rangle f_m \}. \quad (1)$$

Here, $g_m^2 + f_m^2 = 1$, $\hbar\omega_m = 2\pi k_B T(m + 1/2)$ is the Matsubara frequency, Γ is the Dynes parameter, $\gamma = \hbar/2\tau_{\text{imp}}$ is the nonmagnetic-impurity scattering rate, τ_{imp} is the electron scattering time on nonmagnetic impurities, $s = \hbar q v_f / \pi = (q/q_0)\Delta_0$, $\hbar q$ is the superfluid momentum, v_f is the Fermi velocity, $q_0 = 1/\xi_0 = \pi\Delta_0/\hbar v_f$ is the inverse of the BCS coherence length, Δ is the pair potential, Δ_0 is the pair potential of the idealized ($\Gamma \rightarrow 0$) BCS superconductor in the zero-current state ($q = 0$) at $T \rightarrow 0$, θ is the angle between the Fermi velocity and the current, and the bracket $\langle X \rangle$ is the angular averaging of a quantity X over the Fermi surface. We assume a spherical Fermi surface: $\langle X \rangle = (1/2) \int_0^\pi X \sin \theta d\theta$. Note here that considering the average distance the electron travels between electron-nonmagnetic impurity collisions is given by $\ell_{\text{imp}} = v_f \tau_{\text{imp}}$, we obtain the relation $\ell_{\text{imp}}/\xi_0 = \pi\Delta_0/2\gamma$.

In the zero-current state ($q = 0$), the θ dependences of f_m and g_m drop off: $\langle f_m \rangle = f_m$ and $\langle g_m \rangle = g_m$. Then, Eq. (1) reduces to

$$(\hbar\omega_m + \Gamma)f_m - \Delta g_m = 0, \quad (2)$$

which no longer includes the nonmagnetic-impurity scattering rate γ . Hence, in the zero-current state, Δ does not depend on a concentration of nonmagnetic impurities. This robustness of s -wave superconductor to nonmagnetic impurity is known as Anderson's theorem [16].

The Eilenberger equation is compensated by the self-consistency equation

$$\ln \frac{T_{c0}}{T} = 2\pi k_B T \sum_{\omega_m > 0} \left(\frac{1}{\hbar\omega_m} - \frac{\langle f_m \rangle}{\Delta} \right). \quad (3)$$

Here, $k_B T_{c0} = \Delta_0 \exp(\gamma_E)/\pi \simeq \Delta_0/1.76$ is the critical temperature of the idealized ($\Gamma \rightarrow 0$) BCS superconductor, and $\gamma_E = 0.577$ is the Euler's constant. Solving Eqs. (1) and (3) for the current-carrying state or Eqs. (2) and (3) for the zero-current state, we can calculate various physical quantities.

B. Brief review of the consequences of a finite Γ in the zero-current state

Let us briefly review the effects of finite Dynes subgap states on Δ , T_c , and DOS in the zero-current state. Solving Eq. (2), we get

$$g_m = \frac{\hbar\omega_m + \Gamma}{\sqrt{(\hbar\omega_m + \Gamma)^2 + \Delta^2}}, \quad (4)$$

$$f_m = \frac{\Delta}{\sqrt{(\hbar\omega_m + \Gamma)^2 + \Delta^2}}. \quad (5)$$

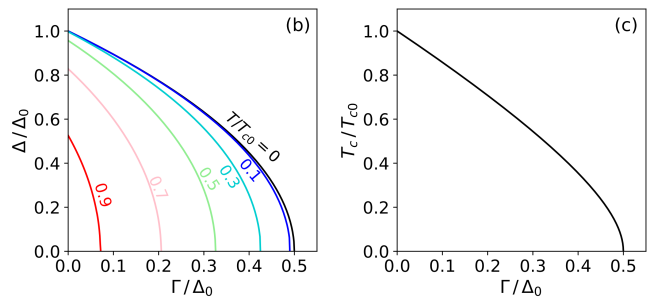


FIG. 2. (a) Pair potential Δ as functions of Γ , calculated for $T/T_{c0} = 0, 0.1, 0.3, 0.5, 0.7$, and 0.9 . (b) Critical temperature T_c as a function of Γ .

Here, $\Delta = \Delta(\Gamma, T)$ is calculated from Eq. (3). For $T \rightarrow 0$, it is easy to find [21, 22, 38, 39, 43, 44, 48]

$$\Delta(\Gamma, T)|_{T \rightarrow 0} = \Delta_0 \sqrt{1 - 2\frac{\Gamma}{\Delta_0}}. \quad (6)$$

Hence, the zero-temperature pair-potential vanishes at the critical value $\Gamma = \Delta_0/2$. Eq. (6) reduces to $\simeq \Delta_0 - \Gamma$ when $\Gamma/\Delta_0 \ll 1$. A calculation for an arbitrary temperature is straightforward. Shown in Figure 2 (a) is Δ as functions of Γ for different temperatures. The larger the temperature is, the smaller the critical value is.

The critical temperature $T_c = T_c(\Gamma)$ is obtained by substituting $T \rightarrow T_c$ and $\Delta \rightarrow 0$ into Eq. (3). We find [21, 22, 38, 39, 43]

$$\ln \frac{T_c}{T_{c0}} = \psi\left(\frac{1}{2}\right) - \psi\left(\frac{1}{2} + \frac{\Gamma}{2\pi k_B T_c}\right), \quad (7)$$

which reduces to $T_c \simeq T_{c0} - \pi\Gamma/4k_B$ for $\Gamma/\Delta_0 \ll 1$. It should be noted that Eq. (7) has the same form as the well-known formula of critical temperature for a superconductor with pair-breaking perturbations [12–16]. Shown in Figure 2 (b) is T_c as a function of Γ , which is a monotonically decreasing function of Γ and vanishes at $\Gamma = \Delta_0/2$.

In the real frequency representation ($\hbar\omega_m \rightarrow -i\epsilon$), we get

$$g(\epsilon) = \frac{\epsilon + i\Gamma}{\sqrt{(\epsilon + i\Gamma)^2 - \Delta^2}}, \quad (8)$$

$$f(\epsilon) = \frac{\Delta}{\sqrt{(\epsilon + i\Gamma)^2 - \Delta^2}}. \quad (9)$$

The quasiparticle DOS is given by $N(\epsilon)/N_0 = \text{Re}[g]$, which corresponds with the Dynes formula shown in Section I (see also Fig 1).

The Dynes Γ is a phenomenological representation of some pair breakers in real materials. Introducing Γ not only yields the broadened DOS (see Fig. 1) but also results in various pair-breaking effects (e.g., suppression of Δ and T_c shown in Fig. 2). In the zero-current state, Δ , T_c , and DOS are independent of a concentration of nonmagnetic impurities (Anderson theorem).

Hence, the results shown in Sec. II B are coincident with those for the dirty limit discussed in the previous studies [21, 22, 38, 39]. In the following sections, we study physical quantities that depend on the Dynes Γ and the nonmagnetic-impurity scattering rate γ .

III. PENETRATION DEPTH AND KINETIC INDUCTANCE

A. Penetration depth

First, consider the penetration depth in the zero-current limit. The penetration depth $\lambda(\gamma, \Gamma, T)$ is calculated from [16]

$$\frac{1}{\lambda^2(\gamma, \Gamma, T)} = \frac{2\pi k_B T}{\lambda_0^2} \sum_{\omega_m > 0} \frac{f_m^2}{d_m}. \quad (10)$$

Here, $\lambda_0^{-2} = \lambda^{-2}(0, 0, 0) = (2/3)\mu_0 e^2 N_0 v_f^2 = \mu_0 e^2 n/m$ is the idealized BCS penetration depth in the clean limit at $T \rightarrow 0$, f_m is given by Eq. (5), and $d_m = \sqrt{(\hbar\omega_m + \Gamma)^2 + \Delta^2 + \gamma}$. Analytical expressions of λ can be obtained for some special cases, e.g., a nearly-ideal ($\Gamma/\Delta_0 \ll 1$) moderately-clean ($\gamma/\Delta_0 \ll 1$) superconductor at $T \rightarrow 0$. The summation can be replaced with integral ($2\pi k_B T/\hbar \sum_{\omega_m > 0} \rightarrow \int_0^\infty d\omega$) when $T \rightarrow 0$, and we find

$$\frac{1}{\lambda^2(\gamma \ll \Delta_0, \Gamma \ll \Delta_0, 0)} = \frac{1}{\lambda_0^2} \left(1 - \frac{\Gamma}{\Delta_0} - \frac{\pi\gamma}{4\Delta_0} \right). \quad (11)$$

Another example is the idealized ($\Gamma \rightarrow 0$) BCS superconductor at $T \rightarrow 0$ including an arbitrary concentration of nonmagnetic impurities. Replacing the summation with integral, Eq. (10) reduces to the well-known formula (see e.g., Ref. [2, 3, 82]):

$$\frac{1}{\lambda^2(\gamma, 0, 0)} = \begin{cases} \frac{1}{\lambda_0^2 \gamma / \Delta_0} \left(\frac{\pi}{2} - \frac{\cos^{-1}(\gamma/\Delta_0)}{\sqrt{1 - (\gamma/\Delta_0)^2}} \right) & (\gamma/\Delta_0 < 1) \\ \frac{1}{\lambda_0^2} \left(\frac{\pi}{2} - 1 \right) & (\gamma/\Delta_0 = 1) \\ \frac{1}{\lambda_0^2 \gamma / \Delta_0} \left(\frac{\pi}{2} - \frac{\cosh^{-1}(\gamma/\Delta_0)}{\sqrt{(\gamma/\Delta_0)^2 - 1}} \right) & (\gamma/\Delta_0 > 1) \end{cases}. \quad (12)$$

In the dirty limit ($\gamma/\Delta_0 = \pi\xi_0/2\ell_{\text{imp}} \gg 1$), substituting $d_m \simeq \gamma$ into Eq. (10), we reproduce the formula derived in the previous study [21]:

$$\begin{aligned} \frac{1}{\lambda^2(\gamma \gg \Delta_0, \Gamma, T)} &= \frac{4k_B T}{\lambda_{0,\text{dirty}}^2 \Delta_0} \sum_{\omega_m > 0} f_m^2 \\ &= \frac{2\Delta(\Gamma, T)}{\lambda_{0,\text{dirty}}^2 \pi \Delta_0} \text{Im}\psi \left(\frac{1}{2} + \frac{\Gamma}{2\pi k_B T} + i \frac{\Delta(\Gamma, T)}{2\pi k_B T} \right). \end{aligned} \quad (13)$$

Here, $\lambda_{0,\text{dirty}}^{-2} = (\pi\Delta_0/2\gamma)\lambda_0^{-2} = \pi\mu_0\Delta_0\sigma_n/\hbar$ is the well-known BCS penetration depth in the dirty limit at $T \rightarrow 0$, and ψ is the digamma function. For the idealized dirty-limit BCS superconductor, Eq. (13) simplifies to [12, 16]

$$\frac{1}{\lambda^2(\gamma \gg \Delta_0, 0, T)} = \frac{\Delta(0, T)}{\lambda_{0,\text{dirty}}^2 \Delta_0} \tanh \frac{\Delta(0, T)}{2k_B T}. \quad (14)$$

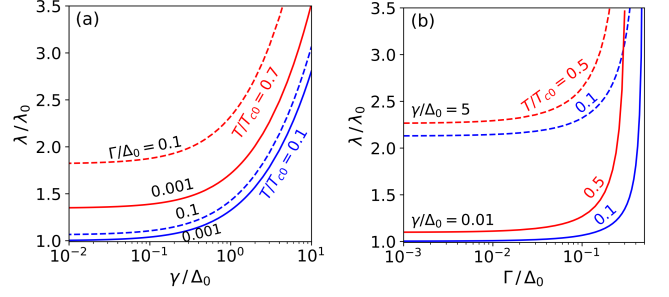


FIG. 3. Penetration depth $\lambda(\gamma, \Gamma, T)$ as functions of (a) nonmagnetic-impurity scattering rate $\gamma/\Delta_0 = \pi\xi_0/2\ell_{\text{imp}}$ and (b) Dynes parameter Γ .

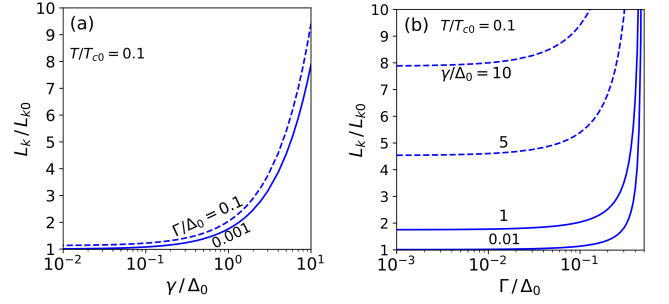


FIG. 4. Kinetic inductivity at $T/T_{c0} = 0.1$ as functions of (a) nonmagnetic-impurity scattering-rate $\gamma/\Delta_0 = \pi\xi_0/2\ell_{\text{imp}}$ and (b) Dynes Γ parameter.

Eq. (14) is widely used when analyzing experimental data of superconducting devices, but its range of applicability is somewhat limited.

To evaluate λ for an arbitrary (γ, Γ, T) , we need to calculate Eq. (10) numerically. Shown in Fig. 3 is λ as functions of (a) γ and (b) Γ for different temperatures: λ is a monotonic increasing function of γ , Γ , and T . The rapid increases of λ at $\Gamma/\Delta_0 \gtrsim 0.1$ come from the pair-breaking effect of Γ close to its critical value (see also Fig. 2 and Ref. [39]).

B. Kinetic inductance

The direct application of the results of Sec. III A is calculations of the kinetic inductance in the zero-current state, which is a crucial physical quantity for superconducting devices, such as KID and SSPD. The kinetic inductance of a thin and narrow film is given by $L_{\text{film}} = [\text{length}/(\text{width} \times \text{thickness})] \times L_k$. Here, L_k is the kinetic inductivity. In the zero-current limit, L_k is given by $L_k = \mu_0 \lambda^2$ (see also Refs. [39, 83, 84] for L_k of a dirty-limit superconductor under the current). Since we have already calculated λ in Sec. III A, we have almost finished the calculations of L_k ; see Fig. 4.

For readers' convenience, let us summarize the analyt-

ical formulas of L_k in the zero-current limit ($q \rightarrow 0$). For a superconductor including an arbitrary impurity concentration, L_k is given by

$$L_k(\gamma, \Gamma, T) = L_{k0} \frac{\lambda^2(\gamma, \Gamma, T)}{\lambda_0^2}. \quad (15)$$

Here, $L_{k0} = L_k(0, 0, 0) = \mu_0 \lambda_0^2 = 3/2e^2 N_0 v_f^2$ is the kinetic inductivity for an idealized ($\Gamma \rightarrow 0$) clean-limit ($\gamma \propto \ell_{\text{imp}}^{-1} \rightarrow 0$) BCS superconductor at $T \rightarrow 0$. In the dirty limit ($\gamma/\Delta_0 = \pi \xi_0/2\ell_{\text{imp}} \gg 1$), taking $d_m \rightarrow \gamma$, we get

$$L_k(\gamma \gg \Delta_0, \Gamma, T) = L_{k0, \text{dirty}} \frac{\lambda^2(\gamma \gg \Delta_0, \Gamma, T)}{\lambda_{0, \text{dirty}}^2}. \quad (16)$$

Here, $L_{k0, \text{dirty}} = \mu_0 \lambda_{0, \text{dirty}}^2 = \hbar/\pi \Delta_0 \sigma_n$ is the inductivity of the idealized ($\Gamma \rightarrow 0$) dirty-limit BCS superconductor at $T \rightarrow 0$. Substituting Eqs. (11) or (12) into Eq. (15) or substituting Eqs. (13) or (14) into Eq. (16), we can analytically evaluate L_k .

It should be noted that, Eqs. (14) and (16) yield the widely-used formula, $L_k = [\hbar \rho_n / \pi \Delta(0, T)] / \tanh[\Delta(0, T)/2k_B T]$, but it can apply only to the idealized ($\Gamma \rightarrow 0$) dirty-limit ($\gamma/\Delta_0 = \pi \xi_0/2\ell_{\text{imp}} \gg 1$) BCS superconductor. The other formulas introduced in this section are more general and would be available for various situations.

IV. COMPLEX CONDUCTIVITY, SURFACE IMPEDANCE, AND Q FACTOR

A. Complex-conductivity formulas

The general formula for the complex conductivity σ of a large- λ/ξ superconductor, which can include an arbitrary concentration of nonmagnetic impurities, is given by [82, 85–88]

$$\sigma(\gamma, \Gamma, T, \omega) = \sigma_1 + i\sigma_2 = \frac{-i\sigma_n}{4\omega\tau} \int_{-\infty}^{\infty} d\epsilon [I_1 \tanh \frac{\epsilon_-}{2k_B T} - I_2 \tanh \frac{\epsilon_+}{2k_B T}], \quad (17)$$

$$I_1 = \frac{g_+ g_- + f_+ f_- - 1}{d_+ + d_-} + \frac{g_+ g_-^* + f_+ f_-^* + 1}{d_+ - d_-^*}, \quad (18)$$

$$I_2 = \frac{g_+^* g_-^* + f_+^* f_-^* - 1}{-d_+^* - d_-^*} + \frac{g_+ g_-^* + f_+ f_-^* + 1}{d_+ - d_-^*}. \quad (19)$$

Here, σ is a function of the impurity scattering rate $\gamma/\Delta_0 = \pi \xi_0/2\ell_{\text{imp}}$, the Dynes parameter Γ , temperature T , and the photon frequency ω ; $\sigma_n = (2/3)e^2 N_0 v_f^2 \tau$ is the dc conductivity in the normal state, τ is the electron relaxation-time, $\epsilon_{\pm} = \epsilon \pm \hbar\omega/2$, $g_{\pm} = g(\epsilon_{\pm})$, $f_{\pm} = f(\epsilon_{\pm})$, $d_{\pm} = d(\epsilon_{\pm})$, and $d(\epsilon) = \sqrt{(\epsilon + i\Gamma)^2 - \Delta^2} + i\gamma$.

In the normal state ($\Delta \rightarrow 0$), we have $g_{\pm} = 1$, $f_{\pm} = 0$, and $d_+ - d_-^* = \hbar\omega + 2i(\Gamma + \gamma)$. Then, Eq. (17) reduces to the Drude model of the ac electrical conductivity of

normal metal: $\sigma_{n1} = \sigma_n/[1+(\omega\tau)^2]$ and $\sigma_{n2} = \sigma_n\omega\tau/[1+(\omega\tau)^2]$ with the electron relaxation-time τ ,

$$\frac{1}{\tau} = \frac{1}{\tau_{\text{imp}}} + \frac{1}{\tau_{\Gamma}}. \quad (20)$$

Here $\tau_{\text{imp}} = \hbar/2\gamma$ and $\tau_{\Gamma} = \hbar/2\Gamma$. It is also possible to derive Eqs. (20) considering a microscopic origin of Γ such as the electron-phonon scattering [87] and electron-magnetic impurities scatterings [43].

In the low-frequency regime ($\hbar\omega \ll \gamma, \Gamma, k_B T, \Delta_0$), we can expand the integrand with respect to a tiny ω . Then, Eq. (17) reduces to

$$\sigma_1(\gamma, \Gamma, T, 0) = \frac{\sigma_n \hbar/\tau}{8k_B T} \int_{-\infty}^{\infty} d\epsilon \frac{1}{\cosh^2(\epsilon/2k_B T)} \left[\frac{(\text{Re } g)^2}{\text{Im } d} + \frac{(\text{Re } d \text{ Im } f - \text{Im } d \text{ Re } f)^2}{\{(\text{Re } d)^2 + (\text{Im } d)^2\} \text{Im } d} \right], \quad (21)$$

and

$$\begin{aligned} \sigma_2 &= \frac{\sigma_n}{2\tau\omega} \int_{-\infty}^{\infty} d\epsilon \tanh \frac{\epsilon}{2k_B T} \text{Re} \left[\frac{f^2}{d} \right] \\ &= \frac{2e^2 N_0 v_f^2}{3\mu_0 \omega} 2\pi k_B T \sum_{\omega_m > 0} \frac{f_m^2}{d_m} = \frac{1}{\mu_0 \omega \lambda^2}, \end{aligned} \quad (22)$$

which are used in Ref. [44] to study the effects of Γ in the low-frequency regime.

In the dirty limit ($\gamma/\Delta_0 = \pi \xi_0/2\ell_{\text{imp}} \gg 1$), we can take $d_+ \simeq d_- \simeq i\gamma$. Then, Eq. (17) reduces to the well-known formulas [85]:

$$\begin{aligned} \sigma_1(\gamma \gg \Delta_0, \Gamma, T, \omega) &= \frac{\sigma_n}{\hbar\omega} \int_{-\infty}^{\infty} d\epsilon [f_{\text{FD}}(\epsilon) - f_{\text{FD}}(\epsilon_{++})] M(\epsilon, \omega), \quad (23) \\ M(\epsilon, \omega) &= \text{Reg}(\epsilon) \text{Reg}(\epsilon_{++}) + \text{Re } f(\epsilon) \text{Re } f(\epsilon_{++}), \end{aligned} \quad (24)$$

and

$$\begin{aligned} \sigma_2(\gamma \gg \Delta_0, \Gamma, T, \omega) &= \frac{\sigma_n}{\hbar\omega} \int_{-\infty}^{\infty} d\epsilon \tanh \frac{\epsilon}{2k_B T} L(\epsilon, \omega) \\ L(\epsilon, \omega) &= \text{Reg}(\epsilon) \text{Im } g(\epsilon_{++}) + \text{Re } f(\epsilon) \text{Im } f(\epsilon_{++}). \end{aligned} \quad (25)$$

Here, $\epsilon_{++} = \epsilon + \hbar\omega$, and $f_{\text{FD}} = [1 - \tanh(\epsilon/2k_B T)]/2$ is the Fermi-Dirac distribution. Eq. (23) is used in Refs. [21, 22, 38] to study the impact of imperfect surfaces on Q factor. It should be noted that, for the idealized ($\Gamma \rightarrow 0$) dirty-limit ($\gamma/\Delta_0 \gg 1$) BCS superconductor, Eqs. (23) and (25) reproduce the textbook formulas [7, 12]:

$$\begin{aligned} \sigma_1(\gamma \gg \Delta_0, \Gamma \rightarrow 0, T, \omega) &= \frac{2\sigma_n}{\hbar\omega} \int_{\Delta}^{\infty} d\epsilon \frac{[\epsilon(\epsilon + \hbar\omega) + \Delta^2][f_{\text{FD}}(\epsilon) - f_{\text{FD}}(\epsilon_{++})]}{\sqrt{\epsilon^2 - \Delta^2} \sqrt{\epsilon_{++}^2 - \Delta^2}} \quad (27) \end{aligned}$$

and

$$\begin{aligned} \sigma_2(\gamma \gg \Delta_0, \Gamma \rightarrow 0, T, \omega) &= \frac{\sigma_n}{\hbar\omega} \int_{\Delta}^{\Delta + \hbar\omega} d\epsilon \tanh \frac{\epsilon}{2k_B T} \frac{\epsilon(\epsilon - \hbar\omega) + \Delta^2}{\sqrt{\epsilon^2 - \Delta^2} \sqrt{\Delta^2 - \epsilon_{--}^2}} \quad (28) \end{aligned}$$

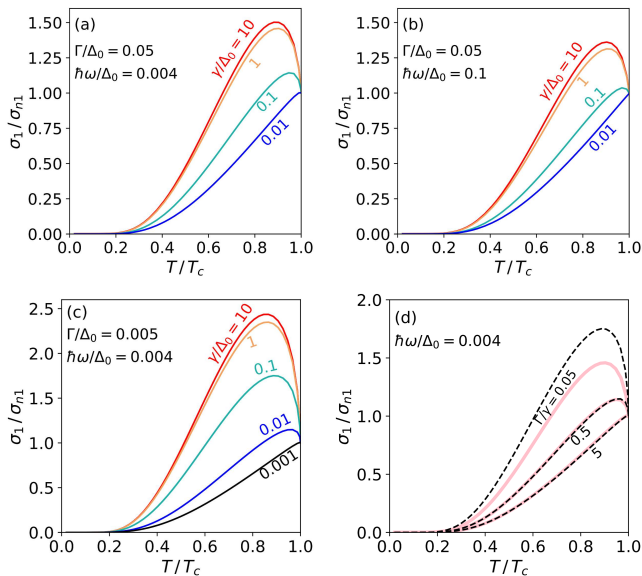


FIG. 5. Temperature dependence of $\sigma_1(\gamma, \Gamma, T, \omega)$. (a) $\Gamma/\Delta_0 = 0.05$ and $\hbar\omega/\Delta_0 = 0.004$. (b) a higher frequency: $\hbar\omega/\Delta_0 = 0.1$. (c) a smaller Dynes Γ : $\Gamma/\Delta_0 = 0.005$. The impurity concentration is varied from $\gamma/\Delta_0 = 0.001$ (clean limit) to $\gamma/\Delta_0 = 10$ (dirty limit). (d) Comparison between (a) and (c). The solid-pink and dashed-black curves correspond to (a) and (c), respectively. The solid and dashed curves for $\Gamma/\gamma = 5$ and 0.5 almost overlap. See also the previous study [44] for the results of $\omega \rightarrow 0$.

for $\hbar\omega < \Delta$. Here, $\epsilon_{--} = \epsilon - \hbar\omega$.

Now, it would be evident that the famous handy-formulas, Eqs. (27) and (28), can apply only to the special case and are usually not enough for quantitative understanding of dissipation in real devices, which generally include some pair breakers. The previous studies used Eqs. (23), (25) and their non-equilibrium version and investigated the effects of Dynes subgap states, strong rf-current, magnetic impurities, and proximity-coupled normal layer at the surface [21, 22, 38, 46]. In the following, we use Eq. (17), which can be applied to a superconductor with an arbitrary impurity concentration, to investigate how a combination of subgap states (Γ) and nonmagnetic impurities (γ) affects σ and Q .

B. Temperature dependence of σ_1 and coherence peak

First, consider the effect of the Dynes Γ and the nonmagnetic-impurity scattering rate $\gamma \propto \xi_0/\ell_{\text{imp}}$ on the temperature dependence of σ_1 and the coherence peak. See also the recent study [44], in which they studied $\sigma_1(T)$ for $\omega \rightarrow 0$.

To examine $\sigma_1(T)$, we need $\Gamma(T)$ too. Here we assume Γ is independent of T for simplicity. Actually, the temperature dependence of Γ depends on its microscopic

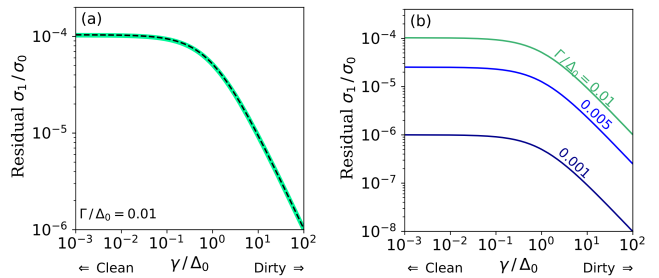


FIG. 6. (a) Residual σ_1 at $T \rightarrow 0$ as functions of the nonmagnetic-impurity scattering rate calculated for $\Gamma/\Delta_0 = 0.01$. The dashed-black curve is the numerical result for $T/T_{c0} = 0.001$ and $\hbar\omega/\Delta_0 = 0.1$. The solid-green curve, which overlaps the dashed-black curve, is calculated from Eq. (29). (b) Residual σ_1 at $T \rightarrow 0$ as functions of the nonmagnetic-impurity scattering rate for different Γ .

origin (e.g., T^3 dependence [42] and constant Γ [43]) and then can depend on materials and surface processing. However, according to experiments so far [48, 89], Γ is nearly constant in some materials. Hence, the T -independent Γ is a somewhat reasonable assumption and would be a good starting point for investigating the temperature dependence of σ_1 .

Shown in Fig. 5 are the temperature dependences of $\sigma_1(\gamma, \Gamma, T, \omega)$ normalized by the real part of Drude's ac conductivity $\sigma_{n1} = \sigma_n/[1+(\omega\tau)^2]$. Fig. 5 (a) is calculated for $\Gamma/\Delta_0 = 0.05$, the photon frequencies $\hbar\omega/\Delta_0 = 0.004$, and several different impurity concentrations. As the material gets clean (as $\gamma/\Delta_0 = \pi\xi_0/2\ell_{\text{imp}}$ decreases), the height of the coherence peak decreases. This result may be counter-intuitive, but it is consistent with the previous theory [44, 87] and supported by experiments [90]. Fig. 5 (b) is calculated for the same Γ as (a) but a higher frequency ($\hbar\omega/\Delta_0 = 0.1$) and shows that ω reduces the height of the coherence peak. Fig. 5 (c) is calculated for the same frequency as (a) but for a smaller Γ , which shows Γ decreases the height of the coherence peak.

Shown in Fig. 5 (d) is the comparison between (a) and (c). Interestingly, as first pointed out in Ref. [44], the temperature dependence σ_1 for a clean-limit superconductor does not depend on Γ and γ separately but on the ratio Γ/γ (see the curves for $\Gamma/\gamma = 5$ and 0.5). Note that this is not the case for a dirty superconductor (see the curve for $\Gamma/\gamma = 0.05$).

C. Residual σ_1 at $T \rightarrow 0$

At $T \rightarrow 0$, it is well-known that σ_1 of the idealized BCS superconductor ($\Gamma \rightarrow 0$) approaches zero. On the other hand, a realistic quasiparticle spectrum expressed with a finite Γ results in a residual σ_1 due to a finite subgap states at the Fermi level [2, 3, 21, 38, 44, 48]. Suppose $\hbar\omega/\Delta_0 \ll 1$. Then, replacing $\tanh(\epsilon/2k_B T)$ with the

Heaviside step function and using $g_{\pm} = \Gamma/\sqrt{\Gamma^2 + \Delta^2}$, $f_{\pm} = \Delta/i\sqrt{\Gamma^2 + \Delta^2}$, and $d_{\pm} = i\sqrt{\Gamma^2 + \Delta^2} + i\gamma$, Eq. (17) reduces to [44]

$$\sigma_1(\gamma, \Gamma, T, \omega)|_{T \rightarrow 0} = \sigma_n \frac{\gamma + \Gamma}{\gamma + \sqrt{\Gamma^2 + \Delta^2}} \frac{\Gamma^2}{\Gamma^2 + \Delta^2}. \quad (29)$$

Here, $\Delta = \Delta(\Gamma, T)|_{T \rightarrow 0} = \Delta_0 \sqrt{1 - 2\Gamma/\Delta_0}$ [see Eq. (6)]. In the dirty limit ($\gamma/\Delta_0 = \pi\xi_0/2\ell_{\text{imp}} \gg 1$), we reproduce [3, 21, 22, 38, 48]

$$\sigma_1(\gamma, \Gamma, T, \omega)|_{T \rightarrow 0} = \sigma_n \frac{\Gamma^2}{\Gamma^2 + \Delta^2}. \quad (30)$$

Note that σ_n depends on electron relaxation time: $\sigma_n \propto \tau$.

Shown in Fig. 6 (a) is the residual dissipative conductivity $\lim_{T \rightarrow 0} \sigma_1$ as a function of the nonmagnetic-impurity scattering rate $\gamma/\Delta_0 = \pi\xi_0/2\ell_{\text{imp}}$. Note that σ_1 is normalized by $\sigma_0 = (2/3)e^2 N_0 v_f^2 \tau_0 = (\tau_0/\tau)\sigma_n$, independent of the electron mean free path of materials in contrast to σ_n . Here, τ_0 is defined by $\tau_0 = \hbar/2\Delta_0$. The dashed-black curve is numerically calculated for $\hbar\omega = 0.1$ and $T/T_{c0} = 10^{-3}$. The solid-green curve, calculated from Eq. (29), overlaps the dashed-black curve and is a good approximation as long as $\hbar\omega \ll \Delta_0$. We find the residual σ_1 decreases as materials get dirty [see Eq. (30): $\sigma_1 \propto \sigma_n \propto 1/\gamma$]. Shown in Fig. 6 (b) is $\lim_{T \rightarrow 0} \sigma_1$ calculated for different Γ using Eq. (29). The residual σ_1 increases as Γ increases (i.e., as subgap states at Fermi level increase). Hence, the subgap-states-induced residual σ_1 can be significantly suppressed by using a nearly ideal ($\Gamma \ll \Delta_0$) dirty-limit ($\gamma/\Delta_0 = \pi\xi_0/2\ell_{\text{imp}} \gg 1$) superconductor.

D. Moderately low-temperature regime ($\hbar\omega \ll k_B T \ll \Delta_0$)

Type-II superconductors used for superconducting devices typically have the gap frequencies $\Delta_0/2\pi\hbar \gtrsim$ a few hundred GHz. Operating frequencies of devices are around ~ 1 -10 GHz and satisfy $\hbar\omega \ll \Delta_0$. The operating temperature depends on the type of device, but almost all devices satisfy $k_B T < 0.2k_B T_c \simeq 0.1\Delta_0 \ll \Delta_0$. Hence, we may consider that a typical operating condition of superconducting microwave devices falls into the category of the low-frequency and low-temperature regime: $\hbar\omega \ll \Delta_0$ and $k_B T \ll \Delta_0$. In particular, when $\hbar\omega \ll k_B T \ll \Delta_0$, σ_1 is mainly determined by thermally activated quasiparticles and is sensitive to the quasiparticle spectrum as shown below.

First, consider the idealized ($\Gamma \rightarrow 0$) BCS superconductor in the dirty limit ($\gamma/\Delta_0 = \pi\xi_0/2\ell_{\text{imp}} \gg 1$). When $\hbar\omega \ll \Delta_0$ and $k_B T \ll \Delta_0$, the main contribution to the integral in Eq. (27) comes from a narrow strip of energy range $0 < \bar{\epsilon} \lesssim k_B T (\ll \Delta)$. Here, we defined $\bar{\epsilon} = \epsilon - \Delta$. Then, the factor $\epsilon^2 - \Delta^2$ reduces to $\simeq 2\bar{\epsilon}\Delta$, the distribution function reduces to $f_{\text{FD}}(\epsilon) - f_{\text{FD}}(\epsilon + \hbar\omega) \simeq$

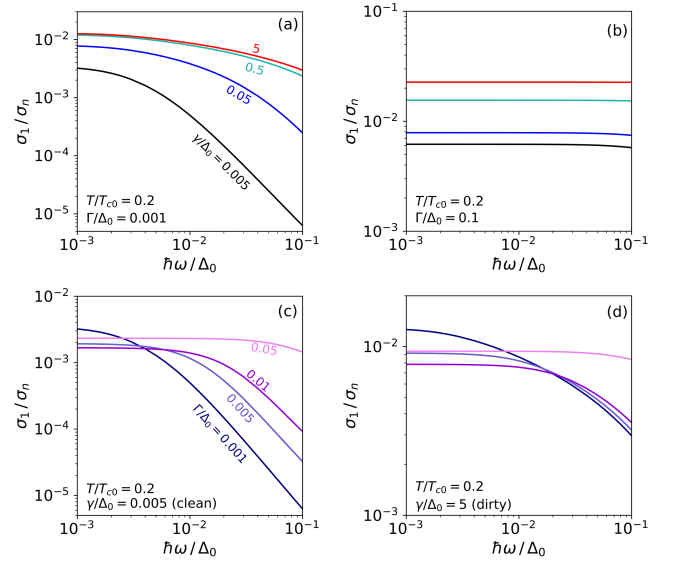


FIG. 7. The dissipative conductivity σ_1 as functions of the photon frequency ω . (a) σ_1 of a nearly-ideal ($\Gamma/\Delta_0 = 0.001$) superconductor calculated for different nonmagnetic-impurity scattering rate $\gamma/\Delta_0 = \pi\xi_0/2\ell_{\text{imp}}$ from the clean limit to the dirty limit. (b) σ_1 of a superconductor with strongly-smearred gap-peaks ($\Gamma/\Delta_0 = 0.1$) calculated for different γ . (c) σ_1 of a clean-limit ($\gamma/\Delta_0 = 0.005$) superconductor calculated for different Dyne Γ . (d) σ_1 of a dirty-limit ($\gamma/\Delta_0 = 5$) superconductor calculated for different Dyne Γ .

$e^{-\Delta/k_B T} e^{-\bar{\epsilon}/k_B T} (1 - e^{-\hbar\omega/k_B T})$, and then Eq. (27) results in the famous handy-formula [3, 5]: $\sigma_1^{\text{dirty}}/\sigma_n = (4\Delta/\hbar\omega) e^{-\Delta/k_B T} \sinh(\hbar\omega/2k_B T) K_0(\hbar\omega/2k_B T)$. Here, the modified Bessel function $K_0(\hbar\omega/2k_B T)$ reduces to $\simeq \ln(4k_B T/e^{\gamma_E} \hbar\omega)$ when $\hbar\omega \ll k_B T$. Hence, we find $\sigma_1^{\text{dirty}} \propto \ln(1/\omega)$. However, as materials get clean, σ_1 exhibits a much different behavior from the dirty limit. Applying the similar calculation as above to Eq. (17), we find $\sigma_1^{\text{clean}} \propto \omega^{-2}$ when $\hbar\omega \ll k_B T \ll \Delta_0$. Fig. 7 (a) shows σ_1 of a nearly-ideal ($\Gamma/\Delta_0 = 0.001$) superconductor as functions of ω for different impurity concentrations from the clean limit (black) to the dirty limit (red). A dirty-limit superconductor (red) exhibits $\ln(1/\omega)$ dependence (see the red curve), while a clean-limit superconductor (black) exhibits ω^{-2} dependence at $\hbar\omega/\Delta \gtrsim 0.01$. The black curve deviates from ω^{-2} dependence at $\hbar\omega \lesssim \gamma$, where the clean-limit assumption is no longer appropriate.

Finite subgap states can drastically change the ω dependence of σ_1 . Fig. 7 (b) is an example calculated for significantly smeared DOS peaks ($\Gamma/\Delta_0 = 0.1$, see also Fig. 1), in which σ_1 is almost independent of ω . Rather than such a large Γ ($\sim k_B T$), a relatively small Γ ($\hbar\omega \lesssim \Gamma \ll k_B T \ll \Delta_0$) induces nontrivial effects. Fig. 7 (c) and (d) are σ_1 for a clean and a dirty superconductor, respectively, calculated for different Γ . In both cases, σ_1 for low-frequency regions ($\hbar\omega \ll k_B T$) decreases as Γ in-

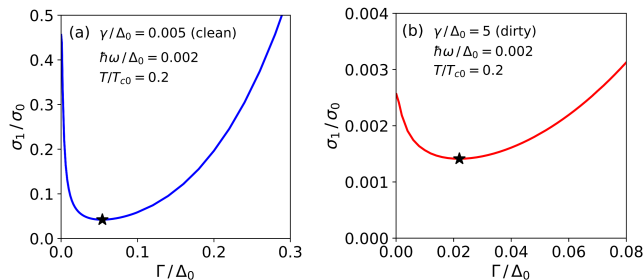


FIG. 8. The dissipative conductivity σ_1 as functions of Dyne Γ . (a) σ_1 of a clean-limit superconductor ($\gamma/\Delta_0 = \pi\xi_0/2\ell_{\text{imp}} = 0.005$) and (b) a dirty-limit superconductor ($\gamma/\Delta_0 = 5$). The black stars are the minimums.

creases, takes the minimum when $\Gamma/\Delta_0 \sim 0.01-0.1$, and then increases with Γ .

Figs. 8 (a) and (b) show σ_1 as functions of Dyne Γ . In both the clean- and dirty-limit cases, the optimum value (Γ_*) minimizes σ_1 . In the clean (dirty) limit, $\sigma_1(\Gamma_*)$ is $\simeq 90\%$ (40%) smaller than that of the idealized ($\Gamma \rightarrow 0$) BCS superconductor. These results can be qualitatively explained as follows. At moderately low temperatures, $\hbar\omega \ll k_B T \ll \Delta_0$, σ_1 is mainly determined by thermally activated quasiparticles and sensitive to the broadening of the DOS. For the dirty limit, the integral of the broadened quasiparticle-spectrum with width $\sim \Gamma > \hbar\omega$ yields $\sigma \propto \log(1/\Gamma)$ [3, 21, 38, 46]. As Γ increases, σ_1 logarithmically decreases [see the slope at $\Gamma \lesssim 0.01$ in Fig. 8 (b)]. In the clean limit, in addition to the broadened quasiparticle-spectrum, the d factor contributes to the integral, resulting in a sharper drop of $\sigma_1 \propto \Gamma^{-1/2} \ln(1/\Gamma)$ [see the slope at $\Gamma \lesssim 0.05$ in Fig. 8 (a)].

According to Eq. (22), we have

$$\sigma_2(\gamma, \Gamma, T, \omega) = \frac{1}{\omega\mu_0\lambda^2(\gamma, \Gamma, T)}, \quad (31)$$

for $\hbar\omega \ll \Delta_0$. Hence the results are already shown in Figs. 3 and 4. Here we do not repeat the calculations of σ_2 . See also Refs. [44, 48].

E. Quality factor and surface resistance

The electromagnetic response of a superconductor is generally nonlocal [17]. However, for an extreme type-II superconductor ($\lambda \gg \xi$), a calculation reduces to a local problem, and the surface impedance Z_s is expressed with the complex conductivity. When $\sigma_1/\sigma_2 \ll 1$ and the thickness of the material is larger than λ , we have

$$Z_s = R_s - iX_s = R_s + jX_s, \quad (32)$$

$$R_s = \frac{1}{2}\mu_0^2\omega^2\lambda^3\sigma_1, \quad (33)$$

$$X_s = \sqrt{\frac{\mu_0\omega}{\sigma_2}} = \mu_0\omega\lambda. \quad (34)$$

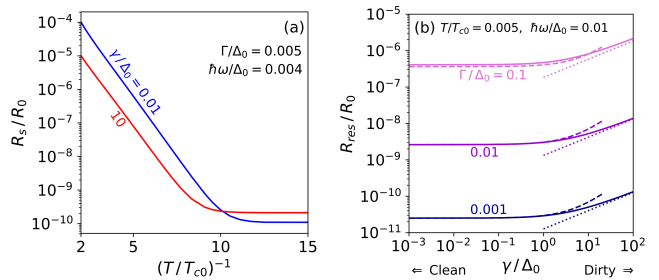


FIG. 9. (a) Surface resistance R_s as functions of $1/T$. Here, Dyne Γ is assumed independent of T for simplicity (see also Section IV B). (b) Subgap-state-induced residual surface-resistance $R_{\text{res}} = \lim_{T \rightarrow 0} R_s$ as functions of nonmagnetic-impurity scattering rate $\gamma/\Delta_0 = \pi\xi_0/2\ell_{\text{imp}}$ calculated for different Dyne Γ . The solid curves are numerically calculated for $T/T_{c0} = 0.005$ and $\hbar\omega/\Delta_0 = 0.01$. The dashed and dotted curves are calculated from Eqs. (38) and (39), respectively.

The quality factor Q can be expressed with these quantities. Remind Q is defined by $Q = \omega U/P$. Here, $P = (1/2) \int R_s |\mathbf{H}|^2 dS$ and $U = (\mu_0/2) \int |\mathbf{H}|^2 dV$ are the dissipation and the stored energy in the cavity, and dS and dV represent the area element and the volume element, respectively. Then, we have $Q = \mu_0\omega \int |\mathbf{H}|^2 dV / \int R_s |\mathbf{H}|^2 dS$, which simplifies to

$$Q = \frac{G}{R_s}, \quad (35)$$

$$G = \frac{\mu_0\omega \int |\mathbf{H}|^2 dV}{\int |\mathbf{H}|^2 dS}, \quad (36)$$

when R_s is uniform on the inner surface of the cavity. We can calculate R_s using the results of Sec.III-IV D and Eq. (33).

Shown in Fig. 9 (a) is R_s as functions of $1/T$ for different impurity concentrations. Here, the normalization factor R_0 is given by

$$R_0 = \frac{1}{2}\mu_0^2\tau_0^{-2}\lambda_0^3\sigma_0 = \frac{\mu_0\Delta_0\lambda_0}{\hbar}. \quad (37)$$

For instances, $R_0 \simeq 0.5\Omega$ and $\simeq 0.8\Omega$ for Nb_3Sn and NbTiN , respectively. At higher temperatures, a dirty superconductor (red) exhibits smaller R_s . At lower temperatures, however, R_s of a clean superconductor (blue) becomes smaller than the red curve. Although the residual σ_1 at $T \rightarrow 0$ decreases as material gets dirtier (see Fig. 6), the contribution from λ^3 significantly pushes up R_s of a dirty superconductor. Shown in Fig. 9 (b) is the subgap-state-induced residual surface resistance $R_{\text{res}} = \lim_{T \rightarrow 0} R_s$ as functions of the nonmagnetic-impurity scattering rate $\gamma/\Delta_0 = \pi\xi_0/2\ell_{\text{imp}}$ (solid curves). R_{res} is a monotonic decreasing function of γ and Γ . For $\Gamma/\Delta_0 \ll 1$ and $\gamma/\Delta_0 \ll 1$ (clean limit), we find an analytical formula of R_{res} for a clean supercon-

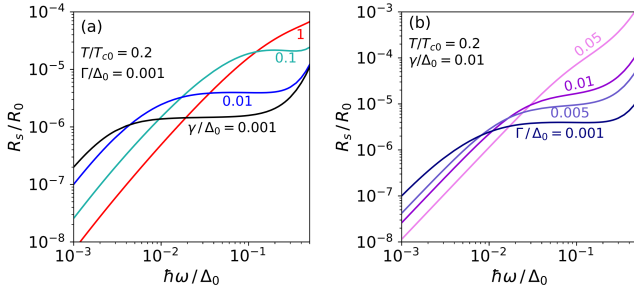


FIG. 10. Frequency dependences of the surface resistance R_s (a) calculated for different nonmagnetic-impurity scattering rate γ and (b) calculated for different Dynes Γ .

ductor:

$$R_{\text{res}}^{\text{clean}} = \frac{R_0}{4} \left(\frac{\hbar\omega}{\Delta_0} \right)^2 \left(\frac{\Gamma}{\Delta_0} \right)^2 \left[1 + \frac{9\Gamma}{2\Delta_0} + \left(\frac{3\pi}{8} - 1 \right) \frac{\gamma}{\Delta_0} \right]. \quad (38)$$

Here, Eqs. (6), (11), and (29) are used. The dashed curves are calculated from Eq. (38), which agree well with the numerical results (solid curves) at $\gamma/\Delta_0 \lesssim 1$. For $\Gamma/\Delta_0 \ll 1$ and $\gamma/\Delta_0 \gg 1$ (dirty limit), using Eqs. (6), (13), and (30), we find

$$R_{\text{res}}^{\text{dirty}} = \frac{R_0}{\pi\sqrt{2\pi}} \left(\frac{\hbar\omega}{\Delta_0} \right)^2 \left(\frac{\Gamma}{\Delta_0} \right)^2 \sqrt{\frac{\gamma}{\Delta_0}} \left[1 + \left(\frac{7}{2} + \frac{3}{\pi} \right) \frac{\Gamma}{\Delta_0} \right]. \quad (39)$$

The dotted curves are calculated from Eq. (39) and agree with the numerical results (solid curves) at $\gamma/\Delta_0 \gtrsim 10$. Here, we have focused on the subgap-state-induced R_{res} , which can be translated into the quality factor $Q_\Gamma = G/R_{\text{res}}$. Note that other factors [e.g., the two-level-system (TLS) defect [91], nonequilibrium quasiparticles [92], and trapped vortices [3]], can also contribute to the total Q :

$$Q^{-1} = Q_\Gamma^{-1} + Q_{\text{TLS}}^{-1} + \dots \quad (40)$$

Suppose $\gamma/\Delta_0 \sim 1$, $R_0 \sim 0.1 \Omega$, and $G \sim 100 \Omega$. Then, $\Gamma/\Delta_0 \sim 0.01$ and 0.1 yield $Q_\Gamma^{-1} \sim 10^{-12}$ and 10^{-10} , respectively. All other contributions need to be suppressed to a level below these values to observe Q_Γ^{-1} .

Next, consider R_s in the moderately-low-temperature regime ($\hbar\omega \ll k_B T \ll \Delta_0$), which corresponds to an operating condition of some types of microwave resonators (e.g., SRF and KID). Fig. 10 (a) shows R_s of a nearly ideal BCS superconductor ($\Gamma/\Delta_0 = 0.001 \ll 1$) as functions of ω calculated for different impurity concentrations. The red curve corresponds to a dirty superconductor, exhibiting the famous ω^2 dependence well below the gap frequency (see, e.g., Ref. [93]). However, as the material gets clean (i.e., as γ decreases), a plateau appears. When $\gamma/\Delta_0 = \pi\xi_0/2\ell_{\text{imp}} = 0.001$ (black curve), R_s is almost independent of ω for a wide frequency range, $0.005 \lesssim \hbar\omega/\Delta_0 \lesssim 0.1$, corresponding to

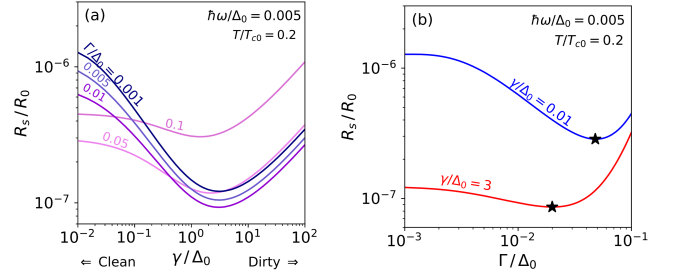


FIG. 11. (a) R_s as functions of nonmagnetic-impurity scattering-rate $\gamma/\Delta_0 = \pi\xi_0/2\ell_{\text{imp}}$ calculated for different Γ . (b) R_s as functions of Γ calculated for $\gamma/\Delta_0 = 3$ (red) and $\gamma/\Delta_0 = 0.01$ (blue). The black stars are the minimums.

$3.7 \text{ GHz} < f < 75 \text{ GHz}$ and $3.4 \text{ GHz} < f < 68 \text{ GHz}$ for Nb_3Sn and NbTiN , respectively. This frequency-independent R_s comes from the ω^{-2} dependence of σ_1 in the clean limit (see Fig. 7) canceling out the ω dependence of $R_s \propto \omega^2 \sigma_1$. Shown in Fig. 10 (b) is calculated for different Dynes Γ . As Γ increases, the plateau shrinks and disappears at $\Gamma/\Delta_0 \sim 0.05$. Only nearly ideal ($\Gamma/\Delta_0 \ll 1$) clean-limit ($\gamma/\Delta_0 \ll 1$) superconductors exhibit the plateau. It should be noted that this result is applicable to extreme type-II superconductors ($\lambda \gg \xi$), while pure Al and pure Nb, which are popular resonator-materials, do not fall into this category.

Now we investigate how to minimize R_s (i.e., maximize Q). Shown in Fig. 11 (a) is R_s as functions of nonmagnetic-impurity scattering rate $\gamma/\Delta_0 = \pi\xi_0/2\ell_{\text{imp}}$. The navy curve is calculated for a nearly ideal BCS superconductor ($\Gamma/\Delta_0 = 0.001$), whose minimum locates at $\gamma/\Delta_0 \simeq 3$, namely, $\ell_{\text{imp}}/\xi_0 \simeq 0.5$. The existence of the optimum mean-free path is very well-known (see, e.g., Ref. [93]); its origin is the interplay of λ^3 and σ_1 , which are increasing and decreasing functions of γ , respectively. As Γ increases, the minimum further decreases (see the dark-violet curve) and then increases at $\Gamma/\Delta_0 \gtrsim 0.01$. Fig. 11 (b) shows this non-monotonic behavior as functions of Γ . The red curve is calculated for a optimally dirty superconductor ($\gamma/\Delta_0 = 3$), reaching the minimum at $\Gamma/\Delta_0 \simeq 0.02$, where R_s is $\simeq 30\%$ smaller than that of the ideal superconductor ($\Gamma \rightarrow 0$) [21, 22, 38, 46]. The blue curve is calculated for a clean superconductor ($\gamma/\Delta_0 = 0.01$). Its minimum locates at $\Gamma/\Delta_0 \simeq 0.05$, where R_s is $\simeq 80\%$ smaller than that of the ideal ($\Gamma \rightarrow 0$) superconductor. The reduction of R_s due to a finite Γ comes from $\sigma_1(\Gamma)$, which is discussed in detail in Sec. IV D [see also Fig. 8].

Remind that we have found that R_s of a clean ($\gamma/\Delta_0 \ll 1$) and nearly-ideal ($\Gamma/\Delta_0 \ll 1$) superconductor can be frequency independent for a wide frequency range (see Fig. 10). For instance, the condition $\gamma/\Delta_0 = \Gamma/\Delta_0 = 0.001$ yields the frequency plateau with $R_s/R_0 \sim 1 \times 10^{-6}$, which is one order of magnitude larger than the global minimum for $\hbar\omega/\Delta_0 = 0.005$ [see the star

on the red curve in Fig. 11 (b)]. However, R_s of such a dirty superconductor increases in proportion to ω^2 and exceeds $R_s/R_0 \sim 10^{-5}$ at $\hbar\omega/\Delta_0 = 0.1$, while a clean and nearly-ideal superconductor on the frequency plateau remains $R_s/R_0 \sim 10^{-6}$ even at $\hbar\omega/\Delta_0 = 0.1$. Moderately dirty ($\ell_{\text{imp}} \sim \xi_0$) superconductors are widely believed to minimize R_s , while the frequency plateau of a nearly-ideal clean superconductor ($\gamma/\Delta_0 \simeq \Gamma/\Delta_0 \simeq 0.001$) can yield much smaller R_s for moderately-high-frequency regions ($\hbar\omega \gtrsim 0.01$) for an extreme type-II superconductor.

V. DEPAIRING CURRENT DENSITY

The depairing current density J_d is the maximum value of the supercurrent density. To obtain J_d , we need to solve Eq. (1) and calculate the current density. The solution for $|q| > 0$ is given by [20]

$$g_m = \frac{a + i \cos \theta}{\sqrt{(a + i \cos \theta)^2 + b^2}}, \quad (41)$$

$$f_m = \frac{b}{\sqrt{(a + i \cos \theta)^2 + b^2}}. \quad (42)$$

Here a , b , $\langle g_m \rangle$, and $\langle f_m \rangle$ are given by

$$\hbar\omega_m + \Gamma + \langle g_m \rangle \gamma - \frac{\pi s}{2} a = 0, \quad (43)$$

$$\Delta + \langle f_m \rangle \gamma - \frac{\pi s}{2} b = 0, \quad (44)$$

$$\langle g_m \rangle^4 + (a^2 + b^2 - 1) \langle g_m \rangle^2 - a^2 = 0, \quad (45)$$

$$\frac{\langle f_m \rangle}{b} = \tan^{-1} \frac{\langle g_m \rangle}{a}, \quad (46)$$

and $\Delta = \Delta(s, \gamma, \Gamma, T)$ satisfies Eq. (3). The current density can be calculated from [16] $\mathbf{J} = -4\pi k_B T e N_0 \text{Im} \sum_{\omega_m > 0} \langle \mathbf{v}_f g_m \rangle$ or

$$\frac{J}{J_0} = -\frac{\sqrt{6}\pi k_B T}{\Delta_0} \sum_{\omega_m > 0} \int_{-1}^1 dc \{c \sin u(c) \sin v(c)\}. \quad (47)$$

Here, $u + iv = \tan^{-1}[b/(a + ic)]$, $c = \cos \theta$, $J_0 = H_{c0}/\lambda_0$, $H_{c0} = \Delta_0 \sqrt{N_0/\mu_0}$ is the thermodynamic critical field of the idealized BCS superconductor ($\Gamma \rightarrow 0$) in the zero-current state, and $\lambda_0 = \lambda(0, 0, 0)$ is the zero-temperature ($T \rightarrow 0$) penetration depth of the idealized ($\Gamma \rightarrow 0$) clean-limit ($\gamma \rightarrow 0$) BCS superconductor in the zero-current state (see also Sec. III A).

Let us briefly review the depairing current density for the idealized ($\Gamma \rightarrow 0$) BCS superconductor. Fig. 12 shows the pair potential Δ and the current density J as functions of the superfluid momentum $q/q_0 = s/\Delta_0$ for the idealized BCS superconductor ($\Gamma \rightarrow 0$) in the clean limit ($\gamma \rightarrow 0$) calculated for different temperatures. When $|q|$ is small, the current pair-breaking effect is limited [Fig 12 (a)], and J linearly increases with $|q|$ [Fig 12 (b)]. However, as $|q|$ increases, the reduction of Δ becomes rapid [Fig 12 (a)], and J ceases to increase [Fig 12 (b)]. The

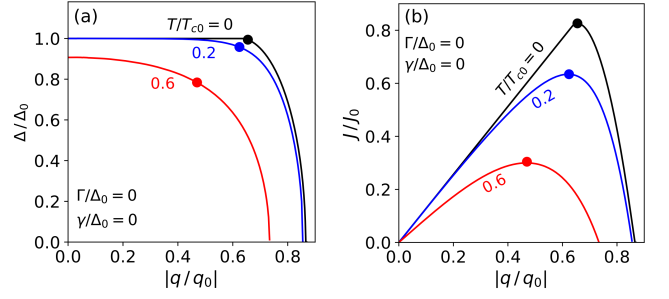


FIG. 12. (a) Δ and (b) J for the idealized BCS superconductor ($\Gamma \rightarrow 0$) in the clean limit ($\gamma = 0$) calculated for $T/T_{c0} = 0, 0.2$, and 0.6 . The blobs correspond to the depairing current densities.

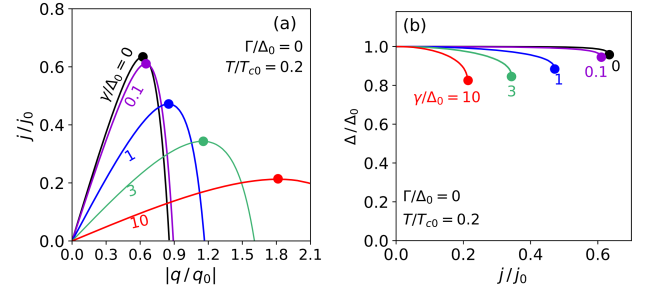


FIG. 13. Effects of impurity scattering-rate γ (See also the previous studies [19, 20]). (a) J as functions of q for the idealized BCS superconductor ($\Gamma \rightarrow 0$) calculated for $\gamma/\Delta_0 = \pi\xi_0/2\ell_{\text{imp}} = 0, 0.1, 1, 3$, and 10 . (b) Δ as functions of J calculated for $J \leq J_d$. The blobs represent the depairing current densities.

maximum value of J (see the blob) is the depairing current density $J_d(\gamma, \Gamma, T)$. Interestingly, when $T/T_{c0} \ll 1$, a finite $|q|$ little affects Δ up to a large momentum close to the depairing momentum. For $\gamma = \Gamma = T = 0$ (i.e., the black curve), the solution is well-known [15, 19, 20]. The pair potential $\Delta = \Delta(s, 0, 0, 0)$ is given by

$$\ln \frac{\Delta}{\Delta_0} = \begin{cases} 0 & (s/\Delta \leq 2/\pi) \\ -\cosh^{-1} \frac{\pi s}{2\Delta} + \sqrt{1 - (2\Delta/\pi s)^2} & (s/\Delta > 2/\pi) \end{cases} \quad (48)$$

and the current density $J = J(s, 0, 0, 0)$ is given by

$$\frac{J}{J_0} = \frac{\pi s}{\sqrt{6}\Delta_0} \begin{cases} 1 & (s/\Delta \leq 2/\pi) \\ 1 - \{1 - (2\Delta/\pi s)^2\}^{3/2} & (s/\Delta > 2/\pi) \end{cases} \quad (49)$$

which reaches the depairing current density,

$$J_d(0, 0, 0) = 0.826 \frac{H_{c0}}{\lambda_0}, \quad (50)$$

at the depairing momentum $q_d/q_0 = s_d/\Delta_0 = 0.655$. According to Eq. (48), Δ is unaffected by the superfluid flow for $q/q_0 = s/\Delta_0 \leq 0.637$, which is very close

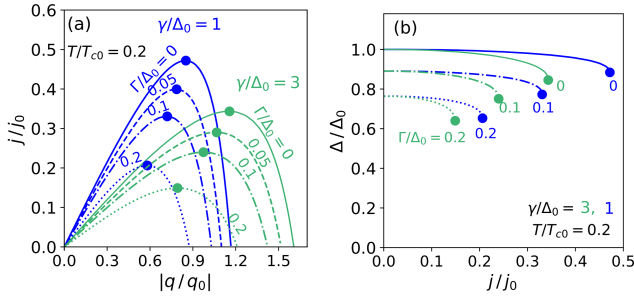


FIG. 14. Effects of Dyson Γ on $J(q)$ and $\Delta(J)$. (a) J as functions of the superfluid momentum q calculated for $\gamma/\Delta_0 = 1$ and 3 and $\Gamma/\Delta_0 = 0, 0.05, 0.1, \text{ and } 0.2$. The blobs correspond to the depairing current densities. (b) Δ as functions of J calculated for $J \leq J_d$.

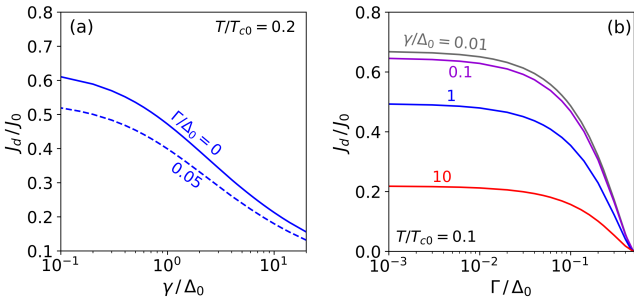


FIG. 15. The depairing current density J_d as functions of (a) the nonmagnetic-impurity scattering rate $\gamma/\Delta_0 = \pi\xi_0/2\ell_{\text{imp}}$ and (b) Dyson Γ parameter.

to the depairing momentum. The nonexistence of current pair-breaking for a broad range of q is the well-known anomalous feature of a clean-limit superconductor at $T/T_{c0} \ll 1$. It should be noted that this feature disappears as T increases (see the red curve); also impure superconductors do not exhibit such an anomalous feature even at $T \rightarrow 0$ (see the dirty-limit results [18, 38, 39, 84] and Fig. 13). Shown in Fig. 13 are $J(q)$ and $\Delta(J)$ of the idealized BCS superconductor ($\Gamma \rightarrow 0$) calculated for different impurity concentrations. As γ increases (as materials get dirty), J_d and $\Delta(J)|_{J \sim J_d}$ decrease: nonmagnetic impurities become pair breakers and significantly impact Δ in the current-carrying state, in contrast to their pair-conserving nature in the zero-current state (see Sec. II B).

Shown in Fig. 14 are the effects of Dyson Γ on $J(q)$ and $\Delta(J)$. As Γ increases, J_d and Δ decrease. In contrast to nonmagnetic impurities, Dyson Γ is always pairbreaking even in the zero-current state as shown in Sec. II B; compare Fig. 13 (b) with Fig. 14 (b).

Fig. 15 (a) shows J_d as functions of the nonmagnetic-impurity scattering rate $\gamma/\Delta_0 = \pi\xi_0/2\ell_{\text{imp}}$; J_d decreases as γ increases (see also Fig. 13). At $\gamma/\Delta_0 \gtrsim 1$, we have $J_d \propto \gamma^{-1/2}$, consistent with the dirty-limit result [18, 38,

39, 84]:

$$J_d(\gamma \gg \Delta_0, \Gamma, T) = C(\Gamma, T) \frac{H_{c0}}{\lambda_{0,\text{dirty}}} \propto \frac{1}{\sqrt{\gamma}}. \quad (51)$$

Here, $\lambda_{0,\text{dirty}} = \sqrt{\hbar\rho_n/\pi\mu_0\Delta_0} \propto \sqrt{\gamma}$ is the zero-temperature penetration depth of the idealized ($\Gamma \rightarrow 0$) dirty-limit BCS superconductor for the zero-current state (see also Sec. III A), and the coefficient $C(\Gamma, T)$ can be calculated from the microscopic theory, e.g., $C(0, 0) = 0.595$ and $C(0, T)$ are calculated some decades ago [18, 19]; $C(\Gamma, T)$ is calculated in Refs. [38, 39]. Fig. 15 (b) shows J_d as functions of Dyson Γ for different impurity concentrations; J_d is significantly suppressed at $\Gamma/\Delta_0 \gtrsim 0.1$, where the pair-breaking scattering almost destroys the superconductivity.

VI. DISCUSSION

The effects of Dyson Γ and nonmagnetic-impurity scattering-rate $\gamma \propto \xi_0/\ell_{\text{imp}}$ on various physical quantities relevant to superconducting devices have been investigated. Here, we summarize our results and discuss their implications for superconducting devices.

A. Kinetic inductance

In Sec. III, we calculated the penetration depth λ and the kinetic inductivity L_k taking the effects of Γ and γ into account and showed that λ and L_k are monotonic increasing functions of Γ and γ (see Figs. 3 and 4). Eq. (11) can evaluate λ for a nearly ideal ($\Gamma/\Delta_0 \ll 1$) and clean ($\gamma/\Delta_0 \ll 1$) BCS superconductor. Eqs. (12)-(14) give other convenient formulas for λ . Combining these formulas with Eqs. (15) and (16), we get the analytical formulas for L_k . Note that Eq. (14) is widely used for analyses of experimental data of superconducting devices, but it is applicable only to the idealized ($\Gamma \rightarrow 0$) dirty-limit ($\gamma/\Delta_0 = \pi\xi_0/\ell_{\text{imp}} \gg 1$) superconductor. To analyze a wide range of materials, Eqs. (11)-(16) or the numerical results (Figs. 3 and 4) would be helpful.

The reset time of SSPD is known to be limited by the kinetic inductance [49], and therefore nanowires with smaller kinetic inductances have been developed. On the other hand, a high kinetic inductance has also attracted attention in the quantum-circuit community; the so-called superinductor makes fluxonium qubit immune to charge fluctuations (see e.g., Ref. [94]). According to our results, not only γ (impurity concentration) but also Γ increase L_k . The effect of Γ on L_k would not be negligible. However, Γ in the material of SSPD, KID, and other quantum circuit is usually not measured. Measurements of Γ of circuit material using tunneling spectroscopy or recently proposed method to extract Γ from complex conductivity, which will be discussed in Sec. VI B, would give insight into a method to engineer L_k .

B. T dependence of σ_1 and coherence peak

In Sec. IV B, we studied the effects of Γ and γ on the T dependence of σ_1 and the coherence peak. The height of the coherence peak decreases as ω or $\ell_{\text{imp}} (\propto \gamma^{-1})$ increases, consistent with the previous theoretical study [44, 87] and experiment [90]. Note that the peak height decreases as the material gets clean. Also, a finite Γ reduces the peak height, consistent with the previous studies for the dirty-limit superconductor [38, 48].

The recent finding of Ref. [44] was also reproduced: the $\sigma_1(T)$ curve for a clean superconductor does not depend on Γ and γ separately but depends on the ratio Γ/γ [see Fig. 5 (d)]. Also, it is possible to extract Γ and γ by fitting experimental data with the theory as proposed in Ref. [44], in which they evaluated Γ and γ using the recent experimental data of SRF resonant cavities [45]. This method would apply to KID and other resonators for quantum technologies. Now, Γ of resonator material can be easily obtained via measurements of σ_1 , which are routinely performed in laboratories. Using experimentally determined Γ , it becomes possible to compare experimental data of devices with the more realistic theories [21, 22, 38, 39] rather than the simplest formulas such as Eqs. (14) and (27).

C. σ_1 and R_s at a very low T

In Sec. IV C and IV E, we calculated the subgap-state-induced residual-dissipative-conductivity $\lim_{T \rightarrow 0} \sigma_1$ and residual surface resistance $R_{\text{res}} = \lim_{T \rightarrow 0} R_s$, which originates from a finite density of subgap states in the vicinity of the Fermi level (see Figs. 6 and 9). Eqs. (29) and (30) are formulas for $\lim_{T \rightarrow 0} \sigma_1$. Also, we derived the formulas for R_{res} , Eqs. (38) and (39), which give good approximations of the numerical results of R_{res} [see Fig. 9 (b)].

These results can be tested by experiments: measure the temperature dependence of σ_1 , extract Γ and γ from $\sigma_1(T)$ using Refs. [44, 45], and cool a resonator down until Q becomes independent of T . However, as shown in Eq. (40), factors other than the subgap-state-induced R_{res} can also contribute to Q . Such contributions should be reduced to a level ignorable as compared with $Q_{\Gamma}^{-1} = R_{\text{res}}/G$, which is typically $< 10^{-10}$ (see Sec. IV E). It would be difficult for a 2D resonator to detect Q_{Γ}^{-1} , in which Q_{TLS}^{-1} always overwhelms Q_{Γ}^{-1} . High- Q SRF cavities [56] may be helpful for this purpose.

D. σ_1 and R_s at a moderately low T

In Sec. IV D and IV E, we studied σ_1 and R_s at moderately-low-temperatures, $\hbar\omega \ll k_B T \ll \Delta_0$.

It was found that σ_1 of a dirty superconductor exhibits the well-known frequency dependence $\propto \ln(1/\omega)$, while that of a nearly-ideal ($\Gamma/\Delta_0 \ll 1$) clean ($\gamma/\Delta_0 = \pi\xi_0/2\ell_{\text{imp}} \ll 1$) superconductor exhibits ω^{-2} dependence

(see Fig. 7), resulting in the frequency-independent surface resistance R_s , shown in Fig. 10. For instance, R_s of a nearly-ideal ($\Gamma/\Delta_0 = 0.001$) clean-limit ($\gamma/\Delta_0 = 0.001$) superconducting resonator made from a large- λ/ξ material (e.g., Nb₃Sn, NbTiN) is frequency-independent between a few GHz and several tens of GHz (e.g., 3.7 GHz $\lesssim f \lesssim 75$ GHz for Nb₃Sn). Roughly speaking, the red curve in Fig. 10 (a) corresponds to a dirty Nb₃Sn cavity operated at $T \sim 4$ K. When the resonant frequency is $f \sim 1$ GHz, which corresponds to $\hbar\omega/\Delta_0 = 10^{-3}$, its surface resistance is $R_s \sim \text{n}\Omega$ from Fig. 10 (a), consistent with experiments. The frequency-independent R_s is realized when the material is nearly ideal and clean (the black curve). R_s of the black curve is one order of magnitude larger than the red curve at $\hbar\omega/\Delta_0 = 10^{-3}$ (~ 1 GHz) but smaller than the red curve at $\hbar\omega/\Delta_0 \gtrsim 10^{-2}$ (~ 10 GHz), where $R_s \sim \mu\Omega$. The red curve increases in proportion to ω^2 , while the black curve remains $R_s \sim \mu\Omega$ even at $\hbar\omega/\Delta_0 \sim 0.1$ (~ 100 GHz). Hence, if there is a demand for a compact cavity with the resonant frequency \sim a few tens GHz, it should be made from a nearly-ideal ($\Gamma/\Delta_0 \ll 1$) clean-limit (γ/Δ_0) type-II superconductor to minimize R_s .

Also, it was found that σ_1 and R_s are non-monotonic functions of Γ , and there exists the optimum value Γ_* which minimizes σ_1 and R_s . For the dirty limit, $\sigma_1(\Gamma_*)$ and $R_s(\Gamma_*)$ are a few tens of % smaller than those of the idealized dirty-limit BCS superconductor, consistent with the previous studies [21, 22]. On the other hand, for the clean limit, $\sigma_1(\Gamma_*)$ and $R_s(\Gamma_*)$ are one order of magnitude smaller than those of the idealized clean-limit BCS superconductor (see Figs. 8 and 11). It has been well-known that the optimum impurity-scattering rate $\gamma/\Delta_0 \sim \xi_0/\ell_{\text{imp}} \sim 1$ minimizes R_s . Such an R_s minimized by the optimum γ can be further reduced by the optimum Γ [see Fig. 11]. These results suggest that we can significantly reduce R_s by tuning Γ . While the physics and materials mechanisms behind Γ are not well understood, comparison of experimentally determined Γ (e.g., using tunneling spectroscopy [23] or complex conductivity measurement [44, 45]) and various materials treatments can give useful information on how to engineer Γ .

E. Depairing current density

In Sec. V, we studied the depairing current density J_d . As shown in Fig. 15, J_d is a monotonically decreasing function of Γ and $\gamma \propto \ell_{\text{imp}}^{-1}$. Hence, we need both Γ and γ to know J_d of the materials of devices or cables. As repeatedly mentioned above, tunneling spectroscopy can determine Γ , and the T dependence of σ_1 [44, 45] can determine Γ and γ . Combining these measurements of Γ and γ with those of J_d , such as Refs. [95, 96], we can test the theory. Also, combining various materials treatments and the Γ measurement can give beneficial information on ameliorating J_d , which is practically important to ex-

amine the quality of superconducting cable and a thin

film laminated on the inner surface of a superconducting heterostructure cavity.

-
- [1] H. Padamsee, 50 years of success for SRF accelerators—a review, *Supercond. Sci. Technol.* **30**, 053003 (2017).
- [2] A. Gurevich, Superconducting Radio-Frequency Fundamentals for Particle Accelerators, *Reviews of Accelerator Science and Technology*, **5**, 119 (2012).
- [3] A. Gurevich, Theory of RF superconductivity for resonant cavities, *Supercond. Sci. Technol.* **30**, 034004 (2017).
- [4] S. Eley, A. Glatz and R. Willa, Challenges and transformative opportunities in superconductor vortex physics, *J. Appl. Phys.* **130**, 050901 (2021).
- [5] J. Zmuidzinas, Superconducting Microresonators: Physics and Applications, *Annu. Rev. Condens. Matter Phys.* **3**, 169 (2012).
- [6] T. M. Klapwijk and A. V. Semenov, Engineering physics of superconducting hot-electron bolometer mixers, *IEEE Trans. Terahertz Sci. Technol.* **7**, 627 (2017).
- [7] J. Zmuidzinas and P. L. Richards, Superconducting detectors and mixers for millimeter and submillimeter astrophysics, in *Proceedings of the IEEE*, **92**, 1597 (2004).
- [8] C. M. Natarajan, M. G. Tanner, and R. H. Hadfield, *Supercond. Sci. Technol.* **25**, 063001 (2012).
- [9] A. Engel, J. J. Renema, K. Il'in, and A. Semenov, *Supercond. Sci. Technol.* **28**, 114003 (2015).
- [10] G. Wendin, *Rep. Prog. Phys.* **80**, 106001 (2017).
- [11] E. Grumblin and M. Horowitz, *Quantum computing: progress and prospects*. (The National Academy Press, Washington DC, 2019).
- [12] M. Tinkham, *Introduction to Superconductivity: Second Edition* (Dover Publications, New York, 2004).
- [13] P. G. De Gennes, *Superconductivity of metals and alloys* (Westview Press, Colorado, 1999).
- [14] A. A. Abrikosov, *Fundamentals of the Theory of Metals* (Elsevier, North-Holland, 1988).
- [15] K. Maki, Gapless superconductivity, in *Superconductivity*, edited by R. D. Parks (Marcel Dekker, Inc., New York, 1969), vol. 2, p. 1035.
- [16] N. B. Kopnin, *Theory of Nonequilibrium Superconductivity* (Oxford University Press, 2001).
- [17] D. C. Mattis and J. Bardeen, Theory of the Anomalous Skin Effect in Normal and Superconducting Metals, *Phys. Rev.* **111**, 412 (1958).
- [18] K. Maki, On persistent currents in a superconducting alloy I, *Prog. Theor. Phys.* **29**, 10 (1963).
- [19] M. Yu Kupriyanov and V. F. Lukichev, Temperature dependence of pair-breaking current in superconductors, *Fizika Nizkikh Temperatur* **6**, 445 (1980).
- [20] F. Pei-Jen and A. Gurevich, Effect of impurities on the superheating field of type-II superconductors, *Phys. Rev. B* **85**, 054513 (2012).
- [21] A. Gurevich and T. Kubo, Surface impedance and optimum surface resistance of a superconductor with an imperfect surface, *Phys. Rev. B* **96**, 184515 (2017).
- [22] T. Kubo and A. Gurevich, Field-dependent nonlinear surface resistance and its optimization by surface nanostructuring in superconductors, *Phys. Rev. B* **100**, 064522 (2019).
- [23] J. Zasadzinski, Tunneling spectroscopy of conventional and unconventional superconductors, in *The Physics of Superconductors*, edited by K. H. Bennemann and J. B. Ketterson (Springer, Berlin, 2003), Vol. 1, p. 591.
- [24] A. Kamlapure, M. Mondal, M. Chand, A. Mishra, J. Jesudasan, V. Bagwe, L. Benfatto, V. Tripathi, and P. Raychaudhuri, Measurement of magnetic penetration depth and superconducting energy gap in very thin epitaxial NbN films, *Appl. Phys. Lett.* **96**, 072509 (2010).
- [25] Y. Noat, V. Cherkov, C. Brun, T. Cren, C. Carbillet, F. Debontridder, K. Ilin, M. Siegel, A. Semenov, H.-W. Hubers, and D. Roditchev, Unconventional superconductivity in ultrathin superconducting NbN films studied by scanning tunneling spectroscopy, *Phys. Rev. B* **88**, 014503 (2013).
- [26] P. Dhakal, G. Ciovati, G. R. Myneni, K. E. Gray, N. Groll, P. Maheshwari, D. M. McRae, R. Pike, T. Proslir, F. Stevie, R. P. Walsh, Q. Yang, and J. Zasadzinski, Effect of high temperature heat treatments on the quality factor of a large-grain superconducting radio-frequency niobium cavity, *Phys. Rev. ST Accel. Beams* **16**, 042001 (2013).
- [27] N. R. Groll, J. A. Klug, C. Cao, S. Altin, H. Claus, N. G. Becker, J. F. Zasadzinski, M. J. Pellin, and T. Proslir, Tunneling spectroscopy of superconducting MoN and NbTiN grown by atomic layer deposition, *Appl. Phys. Lett.* **104**, 092602 (2014).
- [28] C. Becker, S. Posen, N. Groll, R. Cook, C. M. Schlepütz, D. L. Hall, M. Liepe, M. Pellin, J. Zasadzinski, and T. Proslir, Analysis of Nb₃Sn surface layers for superconducting radio frequency cavity applications, *Appl. Phys. Lett.* **106**, 082602 (2015).
- [29] E. M. Lechner, B. D. Oli, J. Makita, G. Ciovati, A. Gurevich, and M. Iavarone, Electron Tunneling and X-Ray Photoelectron Spectroscopy Studies of the Superconducting Properties of Nitrogen-Doped Niobium Resonator Cavities *Phys. Rev. Applied* **13**, 044044 (2020).
- [30] T. P. Devereaux and D. Belitz, Quasiparticle inelastic lifetimes in disordered superconducting films, *Phys. Rev. B* **44**, 4587 (1991).
- [31] D. A. Browne, K. Levin, and K. A. Muttalib, Coulomb-induced anomalies in highly disordered superconductors: Application to tunneling, *Phys. Rev. Lett.* **58**, 156 (1987).
- [32] A. J. Bennett, Theory of the Anisotropic Energy Gap in Superconducting Lead, *Phys. Rev.* **140**, A1902 (1965).
- [33] A. I. Larkin and Y. N. Ovchinnikov, Density of states in inhomogeneous superconductors, *Sov. Phys. JETP* **34**, 1144 (1972).
- [34] A. V. Balatsky, I. Vekhter, and J.-X. Zhu, Impurity-induced states in conventional and unconventional superconductors, *Rev. Mod. Phys.* **78**, 373 (2006).
- [35] J. S. Meyer and B. D. Simons, Gap fluctuations in inhomogeneous superconductors, *Phys. Rev. B* **64**, 134516 (2001).
- [36] R. C. Dynes, V. Narayanamurti, and J. P. Garno, Direct Measurement of Quasiparticle-Lifetime Broadening

- in a Strong-Coupled Superconductor, *Phys. Rev. Lett.* **41**, 1509 (1978).
- [37] R. C. Dynes, J. P. Garno, G. B. Hertel, and T. P. Orlando, Tunneling Study of Superconductivity near the Metal-Insulator Transition, *Phys. Rev. Lett.* **53**, 2437 (1984).
- [38] T. Kubo, Weak-field dissipative conductivity of a dirty superconductor with Dynes subgap states under a dc bias current up to the depairing current density, *Phys. Rev. Res.* **2**, 013302 (2020).
- [39] T. Kubo, Superfluid flow in disordered superconductors with Dynes pair-breaking scattering: Depairing current, kinetic inductance, and superheating field, *Phys. Rev. Res.* **2**, 033203 (2020).
- [40] F. Vischi, M. Carrega, E. Strambini, S. D'Ambrosio, F. S. Bergeret, Y. V. Nazarov, and F. Giazotto, Coherent transport properties of a three-terminal hybrid superconducting interferometer, *Phys. Rev. B* **95**, 054504 (2017).
- [41] G. Tang, W. Belzig, U. Zulicke, and C. Bruder, Signatures of the Higgs mode in transport through a normal-metal-superconductor junction, *Phys. Rev. Res.* **2**, 022068(R) (2020).
- [42] A. A. Mikhailovsky, S. V. Shulga, A. E. Karakozov, O. V. Dolgov, and E. G. Maksimov, Thermal pair-breaking in superconductors with strong electron-phonon interaction, *Solid State Commun.* **80**, 511 (1991).
- [43] F. Herman and R. Hlubina, Microscopic interpretation of the Dynes formula for the tunneling density of states, *Phys. Rev. B* **94**, 144508 (2016).
- [44] F. Herman and R. Hlubina, Microwave response of superconductors that obey local electrodynamics, *Phys. Rev. B* **104**, 094519 (2021).
- [45] D. Bafia, A. Grassellino, M. Checchin, J. F. Zasadzinski, and A. Romanenko, The Anomalous Resonant Frequency Variation of Microwave Superconducting Niobium Cavities Near T_c , arXiv:2103.10601 [physics.acc-ph].
- [46] A. Gurevich, Reduction of Dissipative Nonlinear Conductivity of Superconductors by Static and Microwave Magnetic Fields, *Phys. Rev. Lett.* **113**, 087001 (2014).
- [47] G. Ciovati, P. Dhakal, and A. Gurevich, Decrease of the surface resistance in superconducting niobium resonator cavities by the microwave field, *Appl. Phys. Lett.* **104**, 092601 (2014).
- [48] F. Herman and R. Hlubina, Electromagnetic properties of impure superconductors with pair-breaking processes, *Phys. Rev. B* **96**, 014509 (2017).
- [49] A. J. Kerman, E. A. Dauler, W. E. Keicher, J. K. W. Yang, K. K. Berggren, G. Gol'tsman, and B. Voronov, Kinetic-inductance-limited reset time of superconducting nanowire photon counters, *Appl. Phys. Lett.* **88**, 111116 (2006).
- [50] A. Romanenko, A. Grassellino, A. C. Crawford, D. A. Sergatskov, and O. Melnychuk, Ultra-high quality factors in superconducting niobium cavities in ambient magnetic fields up to 190 mG, *Appl. Phys. Lett.* **105**, 234103 (2014).
- [51] S. Huang, T. Kubo, and R. L. Geng, Dependence of trapped-flux-induced surface resistance of a large-grain Nb superconducting radio-frequency cavity on spatial temperature gradient during cooldown through T_c , *Phys. Rev. Accel. and Beams* **19**, 082001 (2016).
- [52] S. Posen, M. Checchin, A. C. Crawford, A. Grassellino, M. Martinello, O. S. Melnychuk, A. Romanenko, D. A. Segatskov, and Y. Trenikhina, Efficient expulsion of magnetic flux in superconducting radio frequency cavities for high Q0 applications, *J. Appl. Phys.* **119**, 213903 (2016).
- [53] M. Checchin, M. Martinello, A. Romanenko, A. Grassellino, D. A. Sergatskov, S. Posen, O. Melnychuk, and J. F. Zasadzinski, Quench-Induced Degradation of the Quality Factor in Superconducting Resonators, *Phys. Rev. Applied* **5**, 044019 (2016).
- [54] S. Ooi, M. Tachiki, T. Konomi, T. Kubo, A. Kikuchi, S. Arisawa, H. Ito, and K. Umemori, Observation of intermediate mixed state in high-purity cavity-grade Nb by magneto-optical imaging, *Phys. Rev. B* **104**, 064504 (2021).
- [55] D. Longuevergne and A. Miyazaki, Impact of geometry on the magnetic flux trapping of superconducting accelerating cavities, *Phys. Rev. Accel. Beams* **24**, 083101 (2021).
- [56] A. Romanenko, R. Pilipenko, S. Zorzetti, D. Frolov, M. Awida, S. Belomestnykh, S. Posen, and A. Grassellino, Three-dimensional superconducting resonators at $T < 20$ mK with photon lifetimes up to $\tau = 2$ s, *Phys. Rev. Applied* **13**, 034032 (2020).
- [57] S. Posen, A. Romanenko, A. Grassellino, O. S. Melnychuk, and D. A. Sergatskov, Ultralow surface resistance via vacuum heat treatment of superconducting radio-frequency cavities, *Phys. Rev. Applied* **13**, 014024 (2020).
- [58] H. Ito, H. Araki, K. Takahashi, and K. Umemori, Influence of furnace baking on Q-E behavior of superconducting accelerating cavities, *Prog. Theor. Exp. Phys.* **2021**, 071G01 (2021).
- [59] F. He et al. Medium-temperature furnace baking of 1.3 GHz 9-cell superconducting cavities at IHEP, *Supercond. Sci. Technol.* **34**, 095005 (2021).
- [60] R.L. Geng, G. V. Ereemeev, H. Padamsee, and V. D. Shemel'gin, High gradient studies for ILC with single cell re-entrant shape and elliptical shape cavities made of fine-grain and large-grain niobium, in *Proceedings of PAC07, Albuquerque, New Mexico, USA* (2007, JACoW), p. 2337.
- [61] T. Kubo, Y. Ajima, H. Inoue, K. Umemori, Y. Watanabe, and M. Yamanaka, In-house production of a large-grain single-cell cavity at cavity fabrication facility and results of performance tests, in *Proceedings of IPAC2014, Dresden, Germany* (JACoW, CERN, Geneva, 2014), p. 2519. doi:10.18429/JACoW-IPAC2014-WEPRJ022
- [62] A. Grassellino, A. Romanenko, Y. Trenikhina, M. Checchin, M. Martinello, O. S. Melnychuk, S. Chandrasekaran, D. A. Sergatskov, S. Posen, A. C. Crawford, S. Aderhold, and D. Bice, Unprecedented quality factors at accelerating gradients up to 45 MVm^{-1} in niobium superconducting resonators via low temperature nitrogen infusion, *Supercond. Sci. Technol.* **30**, 094004 (2017).
- [63] P. Dhakal, S. Chetri, S. Balachandran, P. J. Lee, and G. Ciovati, Effect of low temperature baking in nitrogen on the performance of a niobium superconducting radio frequency cavity, *Phys. Rev. Accel. Beams* **21**, 032001 (2018).
- [64] A. Gurevich, Enhancement of rf breakdown field of superconductors by multilayer coating, *Appl. Phys. Lett.* **88**, 012511 (2006).
- [65] T. Kubo, Y. Iwashita, and T. Saeki, Radio-frequency electromagnetic field and vortex penetration in multilayered superconductors, *Appl. Phys. Lett.* **104**, 032603 (2014).

- [66] A. Gurevich, Maximum screening fields of superconducting multilayer structures, *AIP Adv.* **5**, 017112 (2015).
- [67] D. B. Liarte, S. Posen, M. K. Transtrum, G. Catelani, M. Liepe, and J. P. Sethna, *Supercond. Sci. Technol.* **30**, 033002 (2017).
- [68] T. Kubo, Multilayer coating for higher accelerating fields in superconducting radio-frequency cavities: a review of theoretical aspects, *Supercond. Sci. Technol.* **30**, 023001 (2017).
- [69] T. Kubo, Superheating fields of semi-infinite superconductors and layered superconductors in the diffusive limit: structural optimization based on the microscopic theory, *Supercond. Sci. Technol.* **34**, 045006 (2021).
- [70] A.-M. Valente-Feliciano, Superconducting RF materials other than bulk niobium: a review, *Supercond. Sci. Technol.* **29**, 113002 (2016).
- [71] S. Posen and D. L. Hall, Nb₃Sn superconducting radiofrequency cavities: fabrication, results, properties, and prospects, *Supercond. Sci. Technol.* **30**, 033004 (2017).
- [72] T. Tan, M. A. Wolak, X. X. Xi, T. Tajima, and L. Civale, Magnesium diboride coated bulk niobium: a new approach to higher acceleration gradient, *Sci. Rep.* **6**, 35879 (2016).
- [73] T. Junginger, S. H. Abidi, R. D. Maffett, T. Buck, M. H. Dehn, S. Gheidi, R. Kiefl, P. Kolb, D. Storey, E. Thoeng, W. Wasserman, and R. E. Laxdal, Field of first magnetic flux entry and pinning strength of superconductors for rf application measured with muon spin rotation, *Phys. Rev. Accel. and Beams* **21**, 032002 (2018).
- [74] C. Z. Antoine, M. Aburas, A. Four, F. Weiss, Y. Iwashita, H. Hayano, S. Kato, T. Kubo, and T. Saeki, Optimization of tailored multilayer superconductors for RF application and protection against premature vortex penetration, *Supercond. Sci. Technol.* **32**, 085005 (2019).
- [75] S. Keckert, T. Junginger, T. Buck, D. Hall, P. Kolb, O. Kugeler, R. Laxdal, M. Liepe, S. Posen, T. Prokscha, Z. Salman, A. Suter, and J. Knobloch, Critical fields of Nb₃Sn prepared for superconducting cavities, *Supercond. Sci. Technol.* **32**, 075004 (2019).
- [76] E. Thoeng, T. Junginger, P. Kolb, B. Matheson, G. Morris, N. Muller, S. Saminathan, R. Baartman, and R. E. Laxdal, Progress of TRIUMF Beta-SRF Facility for Novel SRF Materials, in *Proceedings of SRF2019*, Dresden, Germany (JACoW, CERN, Geneva, 2019), p. 966. doi:10.18429/JACoW-SRF2019-THP047
- [77] H. Ito, H. Hayano, T. Kubo, and T. Saeki, Vortex penetration field measurement system based on third-harmonic method for superconducting RF materials, *Nucl. Instrum. Methods Phys. Res. A* **955**, 163284 (2020).
- [78] Z. Lin, M. Qin, D. Li, P. Shen, L. Zhang, Z. Feng, P. Sha, J. Miao, J. Yuan, X. Dong, C. Dong, Q. Qin, and K. Jin, Enhancement of the lower critical field in FeSe-coated Nb structures for superconducting radio-frequency applications, *Supercond. Sci. Technol.* **34**, 015001 (2021).
- [79] S. Leith, M. Vogel, J. Fan, E. Seiler, R. Ries, and X. Jiang, Superconducting NbN thin films for use in superconducting radio frequency cavities, *Supercond. Sci. Technol.* **34**, 025006 (2021).
- [80] I. H. Senevirathne, A. Gurevich, J. R. Delayen, A. -M. Valente-Feliciano, Measurements of Magnetic Field Penetration in Superconducting Materials for SRF Cavities, in *Proceedings of IPA2021*, Campinas, SP, Brazil (JACoW, CERN, Geneva, 2021), p. 1208. doi:10.18429/JACoW-IPAC2021-MOPAB396
- [81] G. Eilenberger, Transformation of Gorkov's equation for type II superconductors into transport-like equations, *Z. Phys.* **214**, 195 (1968).
- [82] F. Marsiglio and J. P. Carbotte, Electron-phonon superconductivity, in *The Physics of Superconductors*, edited by K. H. Bennemann and J. B. Ketterson (Springer, Berlin, 2003), Vol. 1, p. 73.
- [83] A. J. Annunziata, D. F. Santavicca, L. Frunzio, G. Catelani, M. J. Rooks, A. Frydman, and D. E. Prober, *Nanotechnology* **21**, 445202 (2010).
- [84] J. R. Clem and V. G. Kogan, *Phys. Rev. B* **86**, 174521 (2012).
- [85] S. B. Nam, Theory of electromagnetic properties of superconducting and normal systems. I, *Phys. Rev.* **156**, 470 (1967).
- [86] W. Zimmermann, E. Brandt, M. Bauer, E. Seider, and L. Genzel, Optical conductivity of BCS superconductors with arbitrary purity, *Physica C* **183**, 99 (1991).
- [87] F. Marsiglio, Coherence effects in electromagnetic absorption in superconductors, *Phys. Rev. B* **44**, 5373 (1991).
- [88] D. Rainer and J. A. Sauls, Strong coupling theory of superconductivity, in *Superconductivity: From Basic Physics to the Latest Developments*, edited by P. N. Butcher and Y. Lu (World Scientific, Singapore, 1995), p. 45.
- [89] Szabo et al., Fermionic scenario for the destruction of superconductivity in ultrathin MoC films evidenced by STM measurements, *Phys. Rev. B* **93**, 014505 (2016).
- [90] K. Steinberg, M. Scheffler, and M. Dressel, Quasiparticle response of superconducting aluminum to electromagnetic radiation, *Phys. Rev. B* **77**, 214517 (2008).
- [91] C. Müller, J. H. Cole, and J. Lisenfeld, Towards understanding two-level-systems in amorphous solids: insights from quantum circuits, *Rep. Prog. Phys.* **82**, 124501 (2019).
- [92] P. J. de Visser, D. J. Goldie, P. Diener, S. Withington, J. J. A. Baselmans, and T. M. Klapwijk, Evidence of a nonequilibrium distribution of quasiparticles in the microwave response of a superconducting aluminum resonator, *Phys. Rev. Lett.* **112**, 047004 (2014).
- [93] J. P. Turneaure, J. Halbritter, and H. A. Schwettman, The Surface impedance of superconductors and normal conductors: the Mattis-Bardeen theory, *Journal of Superconductivity*, **4**, 341 (1991).
- [94] D. Niepce, J. Burnett, and J. Bylander, *Phys. Rev. Applied* **11**, 044014 (2019).
- [95] J. Romijn et al., Critical pair-breaking current in superconducting aluminum strips far below T_c , *Phys. Rev. B* **26** 3648 (1982).
- [96] A. Y. Rusanov, M. B. S. Hesselberth, and J. Aarts, Depairing currents in superconducting films of Nb and amorphous MoGe, *Phys. Rev. B* **70** 024510 (2004).